FORECASTING COMPENSATORY CONTROL OF AN PIEZO-ACTUATED MICRO-BORING BAR FOR DYNAMIC ERROR REDUCTION

GAO DONG

M. PHIL.

THE HONG KONG POLYTECHNIC UNIVERSITY

2000

Abstract of thesis entitled
"Forecasting Compensatory Control of an Piezo-actuated Micro-boring Bar for Dynamic Error Reduction"
Submitted by GAO Dong
for the degree of Master of Philosophy
at The Hong Kong Polytechnic University in April 1999

ABSTRACT

In recent years, although significant volume of research work has been devoted to active error compensation in the field of external machining such as turning, milling and grinding, there were only a few attempts that were targeted at overhang boring. In this thesis, the development of a piezoelectric actuated micro-boring bar system with the function of on-line machining error measurement and compensation will be reported.

The sensors used for on-line measuring and compensating the machining error can be easily installed in the tool-post of the machine tool where space is not restricted. Unlike other processes, the implementation of active error compensation for overhang boring poses some real challenge in modern day machine control technology because the conventional sensors which are successful for on-line measurement of the machining errors in external machining are of little use when internal surfaces are encountered. The outer diameter of the boring bar is strictly limited by the size of the bored hole. In order to solve this

problem, a new boring bar consists of two coaxial bars. As a result, the micro-boring bar can be made with smaller outer diameter even after the measuring and compensating sensors have been incorporated.

There are many types of errors effecting the accuracy of the workpiece during the boring operation. In order to compensate the machining errors on-line, a relatively new control strategy, Forecasting Compensatory Control (FCC), is adopted for this boring bar system. The advantage of FCC is its ability to predict the future values of the machining errors without the necessity of solving the complex cause-and-effect relationships between various errors and their sources.

Through the off-line simulation and on-line cutting experiments, the improvement in the roundness accuracy was found to be 39%, and cutting depth accuracy to 60%, which confirms the effectiveness of this proposed strategy.

ACKNOWLEDGMENTS

First of all, I would like to express my acknowledges to the Department of Manufacturing Engineering, The Hong Kong Polytechnic University in providing funding to this research.

I would like to express my sincere gratitude to my chief supervisor, Dr. W. M. Chiu. Thanks for his strong guidance, invaluable advice and continuous encouragement that made this thesis possible. I would also like to thank my co-supervisor, Mr. F. W. Lam, for his suggestions and comments.

I extend my deepest thanks to Prof. Z. J. Yuan of Harbin Institute of Technology, for his valuable ideas and suggests of this research.

I also appreciate Mr. Rico Cheung and Mr. W. H. Luk of the Machine Tools Laboratory for their kindly help in the implementation of the boring bar system. My sincere thanks go to Mr. K. Lee of the Metrology Laboratory for the valuable suggestion for the use of the roundness tester.

I owe many respectful thanks to all my dear friends in the Manufacturing Engineering Department for their thoughtful discussion and assistance.

Last but not least, I thank my parents and sister. I am thankful to my dear wife, LU Ling, for her love, patience, understanding and support of my study.

TABLE OF CONTENTS

LIST OF FIGURES

LIST OF TABLES

Chapter One

INTRODUCTION

1.1 Background

One of the aims of machining processes is to produce a workpiece within the imposed tolerances of shape, dimension and surface quality. However, with the requirements of higher productivity and increased automation, the demand for even greater accuracy and better reliability is becoming more important.

In recent years, information-oriented products, such as computer equipment, optical equipment and communication equipment, have made rapid advances and progress. In order to produce this equipment at higher accuracy, the use of precision and ultra-precision machine tools is rapidly growing. The ultra-precision machine tool, whose machining accuracy is in sub-microns, requires particular techniques different from those of conventional machine tools. With the development of the sensor technology, micro-positioning techniques and modern control techniques, error compensation techniques can now be widely used to improve the machining accuracy in the precision and ultra-precision machine tools [Har90, Don86, Li96, Pat85].

Although a significant volume of research work has been devoted to active error compensation in the field of external machining such as turning [Shi79, Har90, Fan91, Lo95] milling[Lia92, You87] and grinding[Kan76, Ots89], there

are only a few attempts that are targeted at overhang boring under large length/diameter ratios[Hic67, Kim87, Chiu95]. Being the weakest link in the force loop within the machine tool structure, the boring bar alone dominates the overall accuracy and efficiency within the whole machine tool workpiece fixture system [Hah53, Au75].

Unlike other processes, the implementation of active error compensation for overhang boring poses some real challenges in modern-day machine control technology. The sensors used for on-line measuring and compensating the machining error can easily be installed in the tool-heads of an external machining setup where space is not restricted. But, most of these sensors are too large for the boring operation because the outer diameter of the boring bar is constraint by the size of the bored hole. Another major difficulty is due to lack of accessibility of the cutting point which prevents the sensors from being mounted inside the bore for real-time measurement.

Besides, piezoelectric actuators are often employed to provide the active error compensation action. They are known to be well suited to this kind of application, because of their high dynamic response. However, the piezoelectric actuators are sometimes too large to be fitted in the small holes to be bored, preventing them being directly attached to the cutting tool.

Hence, conventional sensors for on-line error measuring and active actuators for error compensation which are successful in many external machining operations are of little use when internal machining operations are encountered.

Though several boring bar systems for on-line active error compensation have been reported [Kim86, Han98, Tan94, Tew95, Sub93]. In these systems, the actuators for error compensation are usually installed inside the boring bar or attached to the cutting tool. Therefore the machining errors are directly measured by laser sensors or capacitor sensors close to the cutting point. However, because of the design, the micro-boring bars produced were often made into a comparatively larger size.

In order to improve the machining accuracy by error compensation methods for the smaller and deeper boring operations, it is necessary to develop a new micro-boring servo system in which the boring bar will have a smaller overall size even after the measuring and compensating sensors have been incorporated.

1.2 Objectives

The overall aim of this thesis work is to develop an on-line compensation control scheme for improving the machining error in the small and deep hole boring operation. The Forecasting Compensatory Control (FCC) method will be used to accomplish this objective.

The general aims and objectives of the project are divided into:

1) To design, fabricate and tune an piezoelectric-actuated micro-boring bar to achieve active compensation of dynamical errors,
2) To study the boring mechanism and machine tool system dynamics to achieve a stable controller for error compensation,

3) To develop, process and measure the real-time error signals with a stochastic model,

4) To develop modeling algorithms to predict step-ahead behaviors of the identified errors,

5) To dynamically compensate for the forecasted errors through controlling the piezo-actuated micro-boring bar and hence,

6) To improve the accuracy of machined surfaces through compensating the measured error signals.

1.3 Contributions and publications

In this thesis, based on a thorough search of the literature, a new boring bar servo system has been successfully developed. The newly developed boring bar was made with a relatively smaller outer diameter. A new control strategy, Forecasting Compensatory Control was adopted in this system to on-line compensate the machining errors during the boring operation. Some results of this project have led to publications as follows:

1 W.M. Chiu, D.Gao, F. W. Lam, and K. W. Chan, "Improvement of Machining Accuracy of Cantilever Boring Bar System Using Piezoelectric Actuator", Trans. of Nanjing University of Aeronautics & Astronautics, 1998, Vol.15, No.1 pp54–58.

2 D. Gao, W. M. Chiu, F. W. Lam, and Z. J. Yuan, "On-line Correction of Form Errors in Precision Micro-boring System by A Compensatory Control

Technique", Proceedings of the Eighth International Manufacturing Conference, Singapore, 12-14th May 1998, pp234-239.

3 W. M. Chiu, D. Gao, F. W. Lam, and Z. J. Yuan "On-line Reducing Machining Errors in Boring Operation by Forecasting Compensatory Control Technique", Proceedings of China Automation Society Conference'98, Hong Kong, 1998, pp38-43.

4 W. M. Chiu, F. W. Lam, and D. Gao, "An Overhung Boring Bar Servo System for On-line Correction of Machining Errors", submitted to Journal of Materials Processing Technology, 2000.

In Paper 1, the principles of the piezoelectric actuator and the error compensation were explained, and the characteristics of the cantilever boring bar and the difficulties encountered in the small & deep hole boring operation were carefully studied. In Paper 2, the mechanical design of the new boring bar was explored in details, and the dynamic model of the boring servo was studied. In Paper 3, the control strategy, Forecasting Compensatory Control (FCC), was successfully developed to on-line model and forecast the machining errors in the boring operation. The advantages of the FCC and the FCC methodology were also discussed. In Paper 4, the dynamic performance of the boring servo was fully analyzed. The on-line cutting experiments have shown that the self-compensatory micro boring bar servo system can greatly improve the machining accuracy.

This project will have a significant industrial potential, demonstrating the approach that can be effective in solving the difficulties faced by many companies

in producing accurate and small diameter bored holes.

1.4 Thesis outline

The contents of the following chapters are briefly explained below.

Chapter 2 reviews the error sources in machine tool operations and the general aspects of machine tool accuracy control, as well as the methods of improving the boring accuracy.

In chapter 3, the implementation of the micro-boring system is discussed. Mechanical design and electronic design of the boring system are explained in detail. Also, the performances of the boring bar are verified through experiment.

Chapter 4 presents the mathematical and conceptual essentials of stochastic modeling, forecasting and the control algorithm. Also, for on-line control, recursive parameter estimation methods are presented.

Chapter 5 describes the control algorithm, Forecasting Compensatory Control (FCC), used for the on-line control system. This whole system control structure and features are also discussed.

Chapter 6 will give the experimental procedures for evaluating the system capabilities.

Chapter 7 will give the conclusion of the project and the future work needed to be done.

Chapter Two

LITERATURE REVIEW

This chapter deals with the general aspects of the machine tool accuracy and its control. The first part of the chapter describes the error source and its classification in machine tool operations for the purpose of understanding the diversity and variability of machine tool errors, and the complexity of the problem of achieving high form and dimensional accuracy. The second part outlines the methodology to improve the machining accuracy. Lastly, the traditional methods of active error compensation used in the operations of turning, milling, boring etc. are also introduced.

2.1 Machining Errors in Machine Tool

2.1.1 Error sources

Errors in a machine tool operation originate from many sources such as quasi-static machine tool errors, dynamic machine tool errors, workpiece and tooling errors, etc [Kim86, Cha93]. The effects and relationships of all error sources are shown in Fig. 2.1.

Quasi-static machine tool errors are those errors of relative position between the tool and the workpiece that are slowly varying in time and are related to the structure of the machine tool itself. These errors may be divided into four general

classes:

i. those due to the geometry of the machine,

ii. those due to static and slowly varying forces such as dead weight of the machine components, over-constrained slides, workpiece weights, and the like,

iii. those due to the thermally induce strains in the machine tool structure, and

iv. those due to kinematics of machine.

Dynamic machine tool errors are associated with the dynamic behavior of the machine tool. These errors may be divided into three general classes: those due to the cutting process heat, those due to both forced and self-induced vibrations, and those due to deformation by cutting force.

Heat created by the cutting process causes a temperature rise between the tool and the workpiece, chip generation and coolant. Forced vibrations are found without exception in all machining operation. Inherent sources of forced vibrations include unbalanced rotating masses in the machine tool drives, gears and bearings, reciprocating elements, unbalanced electric motors, oil pumps, etc. Self-excited vibration, commonly called "chatter", would take place when the frequency of the external force is close to the system's natural frequency. Deflections of cutter and workpiece produced by the cutting force during machining also result in form and dimensional inaccuracy on the finished workpiece. Often, form errors are caused by variations of cutting force during the cutting process, which come either from the initial form error of workpiece or the

variations of stiffness of both workpiece and machine tool.

Besides the errors that can be associated with the machine tool itself, there is a class of errors that are more closely related to the workpiece, the cutting tool or the interaction between the two, such as tool wear, tool setting, chucking and fixture, material stability, etc.

By considering all these error sources and their complicated relationships, it can be realized that the problem of machining accuracy is extremely complicated due to the diversity and variability of the machining process and the difficulties involved in machining accuracy control.

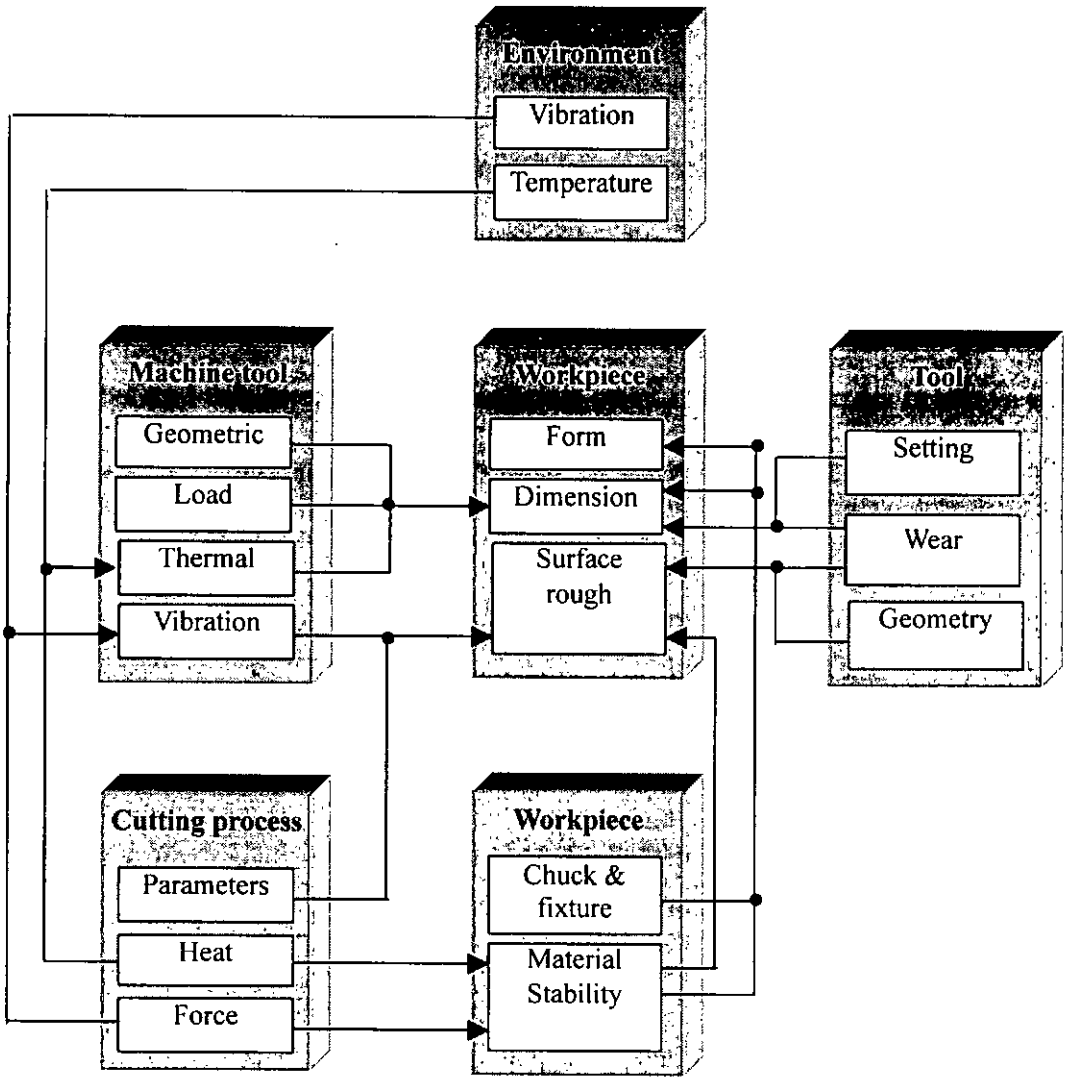

Fig. 2.1 Factors influencing machining accuracy

2.1.2 Classifications of machining errors

From the analysis above, it is indicated that the machining errors are complicated and diversified. According to their characters, the machining errors can be divided into two main categories [Wu89]: systematic errors and stochastic errors. In general, the systematic errors are often due to the orderly error sources such as the geometry of the machine, the cutting force deformation, tool wear etc. Among the systematic errors, some are simple and expressible, others are complicated and inexpressible. The classification of machining errors is shown in Fig.2.2.

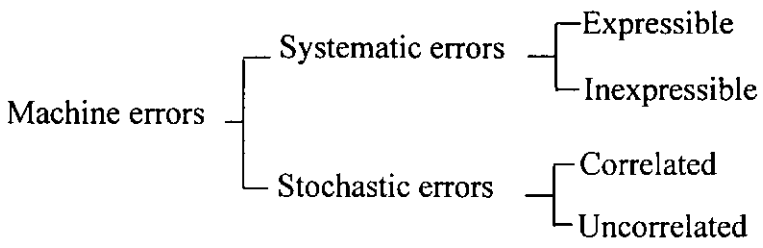

Fig. 2.2 Classification of machine errors

2.2 Machine Tool Accuracy Control

There are a number of strategies to reduce the errors that lower the accuracy of a machine tool. In general, these strategies can be divided into two categories, namely "error avoidance" and "error compensation"[Ras92].

2.2.1 Error avoidance

Error avoidance collectively refers to those techniques, which build the accuracy into machine tools by minimizing the sources of inaccuracy during the

design and manufacturing phases. The following systems and technologies are error avoidance frequently employed to improve machine tool accuracy:

1) Good vibration isolation systems and materials such as synthetic granite,
2) Precision temperature and humidity control system,
3) Precision feed drive system such as backlash-free preloaded ball-nut and screw system with a low-inertia servomotor and a high resolution feedback sensor,
4) Straight low friction slide-way with anti stick-slip properties,
5) Air- or hydrostatic- bearing systems, hydrostatic spindle bearings, and efficient cooling systems for thermal stability of the structure,
6) High precision rotating spindles and guide-ways, and
7) Coaxial-motor technique, the spindle and the driver motor are directly connected without any other transmission elements.

With these approaches, machine tool costs rise sharply with the level of accuracy desired. Furthermore, in many instances such as boring, the scope of improvement by the error avoidance approach is severely restricted by the job requirements and by the finite material properties of the machine tool structure. Considering that the cost of the error avoidance method rises steeply with the accuracy level desired for industries demanding more accurate products, the cost of implementing error avoidance often becomes too high for economical production. A more economical and perhaps more practical approach to this inaccuracy problem can be achieved by the second approach, i.e., error correction.

2.2.2 Error compensation

The error compensation method is based on the measurement and correction of errors by means of a) pre-calibrated error compensation or b) active error compensation. The former refers to a technique used to measure errors before or after a machining process and to use the measured errors for calibrating or altering the process during subsequent operations. While several pre-calibrated compensation schemes[Chi59, Hoc80, Fer87, Asa92] which are mainly for static errors have been developed and successfully implemented, the pre-calibrated compensation of error approach is founded on the assumption that the machining system can be regarded as time-invariant with insignificant parameter variation. As a machining process is unavoidably influenced by a number of factors, a major disadvantage of this technique is found in its lack of robustness and inability in controlling random factors arising from the machining process.

Active error compensation occurs when an error is monitored during the machining operation. It assumes that the measuring system is repeatable and accurate. Active error compensation is distinguished from pre-calibrated error compensation by two characteristics. Firstly, the measurement of error and compensation thereof occur simultaneously in active compensation. Secondly, active error compensation depends on the repeatability or stability of the measurement system only. If a non-repeatable error were to occur somewhere in the machining process, active compensation would sense this and act accordingly.

Undoubtedly, active error compensation is the most effective and reliable

method to deal with dynamic factors such as non-uniform depths of cut, spindle motion error and machine vibration etc[Che98, Gro90]. Over the years, real-time error compensation has received widespread attention due to its ability to correct machine errors with sound cost effectiveness. A very large volume of work has been reported in areas such as Huang's work [Hua84] in roundness control for grinding, Kim's [Kim85] in cylindricity for in-line boring, Sun's [Sun86] in gear grinding, Okazaki's [Oka90] and Lo's [Lo95] in turning, Wang's [Wan94] in cylindricity for precision turning.

2.2.3 FCC techniques

Along the direction of active error compensation, a new approach called Forecasting Compensatory Control (FCC) has been under development for the past twenty years. This new method makes full use of advanced on-line sensing, computing, stochastic modeling, and control actuating techniques. Its major feature is that the method not only compensates for repeatable, systematic errors, but also provides a way to forecast the non-repeatable stochastic errors so that correlated dynamic errors can also be corrected. The key to this new approach is the use of on-line stochastic modeling.

FCC is not merely a control algorithm, but a complete compensatory control scheme. There are five essential parts of this FCC technique [Wu89, Par88]: in-process error measurement, on-line signal processing, stochastic modeling, forecasting and compensatory control. For different applications, these basic

aspects may be different.

(1) In-process error measurement:

Only in-process error measurement offers potential for the compensatory control of both repeatable and non-repeatable components of machining errors. Compared with off-line measurement method, the in-process method has the following obvious advantages: its results are closer to the actual machining situations, and it can continuously monitor the variation of a process.

(2) On-line signal processing

Because most of the in-process measurements use indirect methods, it is necessary to analyze the measured results and to obtain a relation between the measured results and the equivalent errors at a compensation point. The errors at this compensation point can then be estimated. After processing, only these errors at the compensation point need be monitored. One basic requirement of the processing algorithm is its real-time processing speed.

(3) Stochastic modeling

Any physical process has its own dynamics. That is, the current behavior of a process variable is affected by the combination of its past behaviors and some new external causes. Stochastic models are employed in the FCC techniques to adequately describe the dynamic process. A properly established stochastic model

of a process variable not only can describe the dynamic variable, but also can predict the future values of that variable based on its current value.

(3) Forecasting

One of the most important features of the FCC technique is its forecasting capability. Based on the past and current measurements as well as the developed stochastic model, the behavior of errors at a compensation point will be predicted before a cutter actually cuts at the point. This forecasting function overcomes the time lag between the moment of measurement and of taking control action. It gains extra time for a controller to generate compensatory commands and for a actuator to properly respond.

(4) Compensatory control

After a forecast of the errors is made, compensatory action will be taken. In this aspect of the FCC techniques, the basic requirement is how to accurately respond to a compensation command. It frequently needs the development of new actuators, such as piezoelectric actuating devices, to achieve the desired response. The objective of this compensatory control is to maintain some output variable, such as machining form accuracy, as close to its target value as possible when a system is subjected to disturbances. The minimum variance control is often used in the FCC techniques.

2.3 Typical Micro-positioning Devices

The micro-positioning device is one of the key parts in the machine tool with a function of active error compensation. Several typical devices with piezoelectric actuator are introduced below:

Fig.2.3 shows the tool drive designed by Your [You87]. It is composed of an piezoelectric actuator, parallel-spring stage, and a capacitance gap sensor. One end of the piezoelectric actuator is connected to the tool body by one magnetic cylinder, and the other end is fastened on the tool shank. As a high voltage is supplied to the actuator, it will expand and push the tool shank and diamond tool. The actual tool displacement is detected by the position sensor which can sense the gap between the flat plate and sensor probe. The parallel-spring stage is functioned to move the tool shank parallel and to support the flat plate overhead for the tool position measurement.

Fig.2.4 shows the micro-cutting device designed by Hara [Har90]. It consists of a pair of parallel springs, two piezoelectric elements (one for driving and the other for contact detection) and a diamond tool. A capacitance gauge, measuring the distance between the workpiece and the tool, is mounted on it. A pair of parallel springs is arranged symmetrically so that a tool base, placed between the springs, may move exactly in the horizontal direction. Each parallel spring, consisting of 8 notches, is formed by means of a wire cut electric discharge machine from a steel block.

Fig.2.5 shows the micro-cutting device developed in Harbin Institute of

Technology [Wan94]. In this tool drive, an electrostrictive actuator is employed for active error compensation. One end of the piezoelectric actuator is connected to the moving part of the cutting device, and the other end is connected to a screw through a steel ball protecting the piezoelectric actuator from a shear force.

In these three micro-feed cutting devices, displacement actuators and cutting tools lie in a line, and the dimension of the cutting device is larger in the cutting direction. Hence, the design of these kinds of cutting device is not convenient for internal face machining.

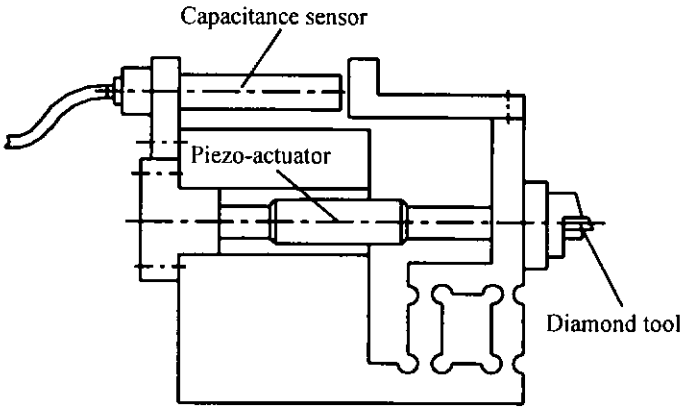

Fig.2.3 Tool drive designed by S.B. Your

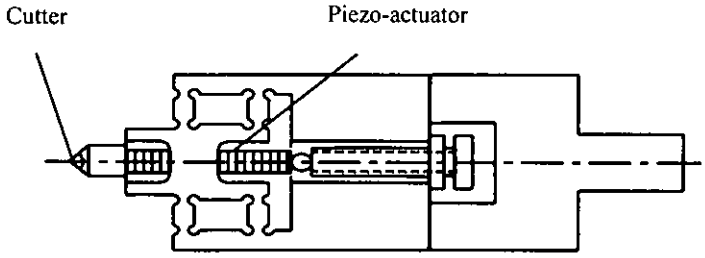

Fig.2.4 Micro cutting device developed by Y. Hara

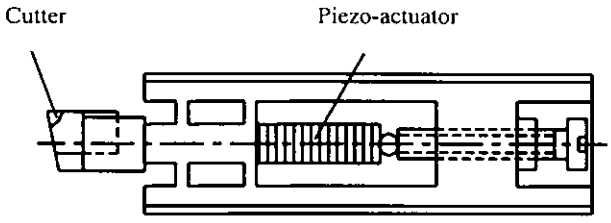

Fig.2.5 Cutting drive developed in Harbin Institute of Technology

2.4 Methods to Improve Boring Accuracy

In the case of boring bars, owing to their large length to diameter ratios and the associated low dynamic stiffness at resonance, force-induced errors can easily develop during cutting operation. To improve their performance, a large volume of research work has been reported. The following outlines some significant work reported before.

Stiffness, mass and damping are the determinant factors on the dynamic performance of the boring bar. Two basic ways to improve performance of a boring bar are enhancement of its stiffness and damping. Stiffness of the boring bar can be increased by using high Young's modulus materials such as sintered carbides. However, such materials and their fabrication are very costly. So dampers and vibration absorbers are frequently used to increase the damping of the system.

Another approach is the application of a combination structure. As shown in Fig.2.6, a boring bar which adopts a combination structure with tuned dynamic vibration absorber is developed by Rivin [Riv89] to improve the dynamic performance of a cantilever boring bar. In the boring bar, the root segment of the cantilever is made of material having a high Young's modulus to increase its effective stiffness and the free end segment is designed to be light to reduce its effective mass. In this design, natural frequencies are increased and effective mass is reduced without a significant reduction of stiffness. The latter factor leads to an increase in the mass ratio of the absorber, especially considering the limited space

inside the bar and thus a limited size of the inertia weight, resulting in an improved absorber effectiveness and dynamic performance. It is an error avoidance method to improve the machining accuracy.

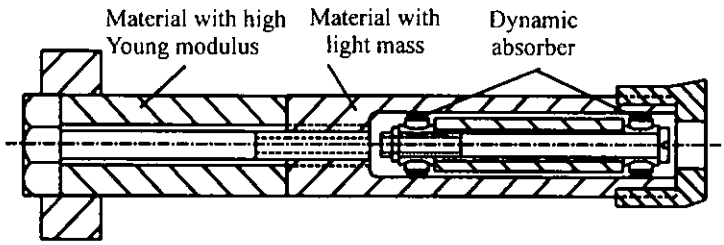

Fig.2.6 Multi-structural boring bar with dynamic absorber

An error compensation method is employed to improve the machining accuracy of the boring bar. As shown in Fig. 2.7, a noble hollow boring device using a laser beam and a lateral photo-sensor feedback was adopted by Kim [Kim87] to compensate active errors during the boring process. While this setup was largely successful in correcting errors for relatively larger holes, the need of a hollow bar to accommodate an actuator, prism etc., makes it unsuitable for use in smaller bores.

In order to avoid the actuator sensors affecting the size of the boring bar, Hanson [Han94] developed a boring servo system useful for variable-depth-of-cut machining. As shown in Fig.2.8, in this system, a flexural hinge is employed to convert the actuation of the piezoelectric actuator in axial direction into the radial direction, making the size of the boring bar not affected by the piezoelectric actuator. However, as a proximity sensor is used for measuring the position of the cutting tool during the boring process, this boring bar has to be made a

comparatively larger size as the position sensor is mounted.

To bore small and deep holes, a boring bar for on-line active form error compensation has been developed in the Hong Kong Polytechnic University (HKPolyU) [Chiu97]. As shown in Fig.2.9, the boring bar was built up in a lever structure with the cutting tool and piezoelectric actuator installed into the two ends of the bar, and two strain gauges were attached to the root segment of the bar for cutting force measurement during the boring process. The boring bar which is not affected by the piezoelectric actuator and the strain gauges could be made of comparatively smaller size. The boring system adopted an open-loop PID control model based on the force-induced control. Though this attempt has met with considerable success in compensating real-time errors, a finite time delay exists between a measurement and control action. Therefore some form of forecasting of future errors is desirable to account for the time lag.

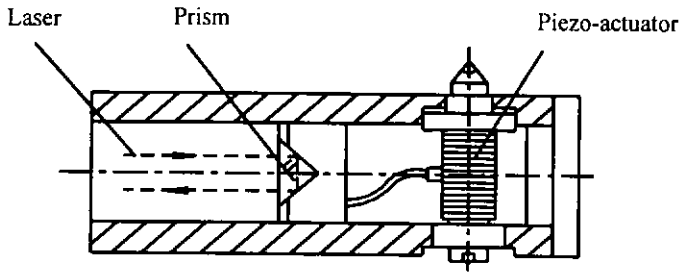

Fig.2.7 Kim's micro-boring bar used for error compensation

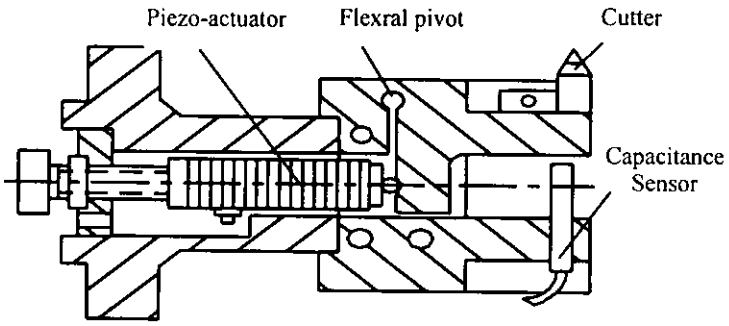

Fig. 2.8 Hanson's micro-boring bar used for error compensation

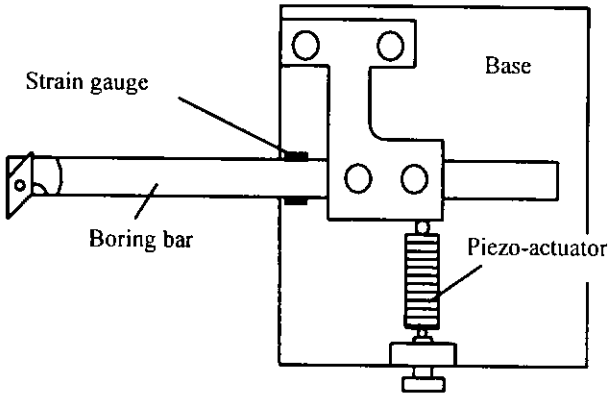

Fig. 2.9 The micro-boring bar in the HKPolyU

Chapter Three

IMPLEMENTATION OF MICRO-BORING SYSTEM

Active error compensation has been widely used in the field of external machining. The sizes of those cutting devices are not restricted in general, therefore, the on-line measuring gauge and compensating actuator can be conveniently installed. Unlike the external machining, the implementation of active error compensation for over-hang boring poses a real challenge because suitable gauges for error measurements are practically non-existent for monitoring boring in smaller holes. Besides piezoelectric actuators, which are often employed in the active error compensation system, are sometimes too large to be fitted in the small holes to be bored preventing them being directly attached to the cutting tool. Hence most conventional sensors and active actuators which are successful for real-time measurement and compensation in external machining are of little use when internal surfaces are encountered. In order to improve the machining accuracy of the small and deep hole boring operation, a new structural micro-boring servo system is to be developed, in which the boring bar has a smaller outer size and larger length.

3.1 Experimental Setup

The experimental setup was arranged on a CNC lathe (MAZAK QUICK TURN 8N). The photograph of the experimental setup is shown in Fig. 3.1. The schematic arrangement of the experimental setup is shown in Fig. 3.2. It is composed of micro-boring bar, strain gauge error measuring meter, control computer, piezoelectric actuator and its power amplifier, A/D and D/A converter, and a low-pass filter. The boring bar was designed with a new structure consisting of two concentric bars, the outer one is used for error compensation and the inner for error measuring.

As shown in Fig.3.2, the compensation bar adopts a lever structure with a piezoelectric actuator and boring cutter installed at the two ends of the bar respectively. The displacement of the piezoelectric actuator can be transferred into the micro-feeding of the boring cutter by driving the control bar to rotate around the flexural pivot. The measuring bar is of a cantilever structure with two strain gauges attached for measuring the machining error. The micro-feeding of the boring cutter was indirectly obtained through measuring the deflection of the measuring bar by the strain gauges. As a result, the micro-boring bar can be made with a relatively smaller outer diameter even after the piezoelectric actuator and strain gauges have been incorporated.

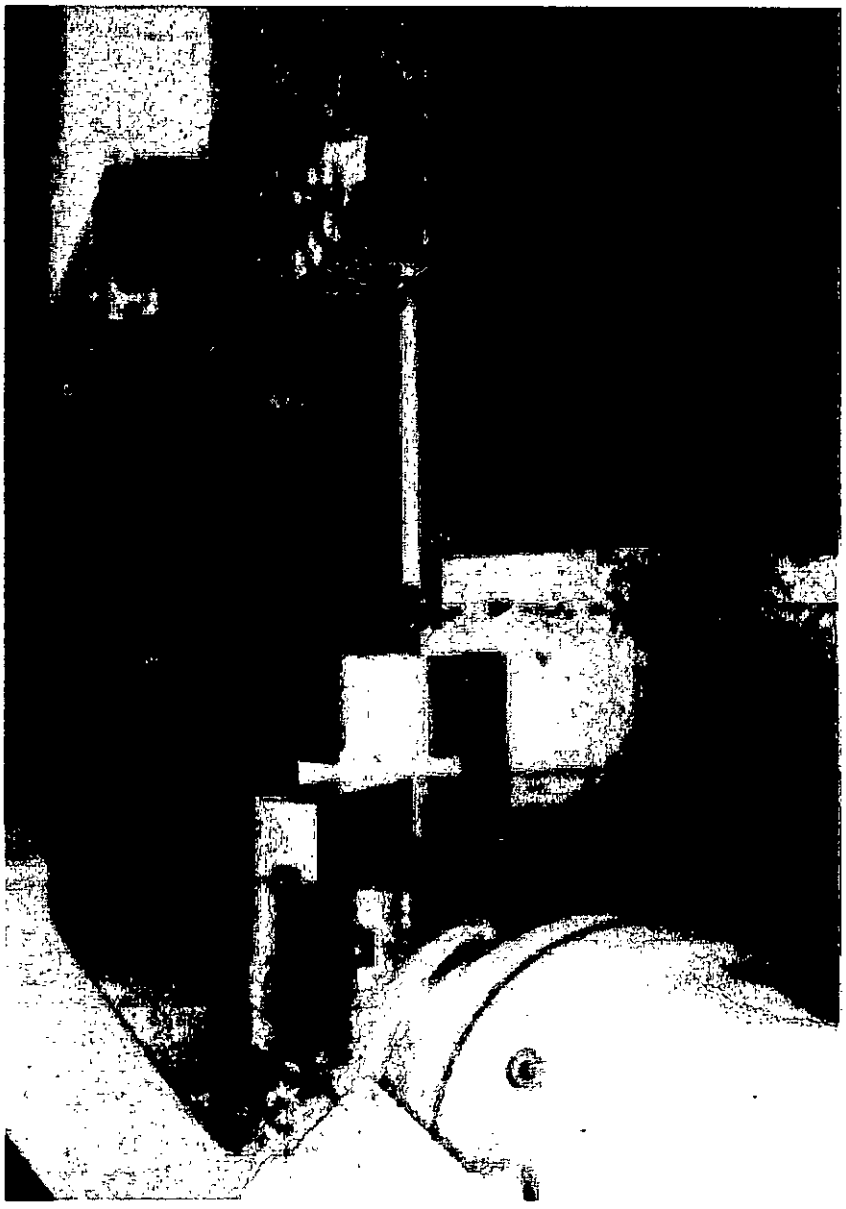

Fig. 3.1 the photograph of the boring bar system

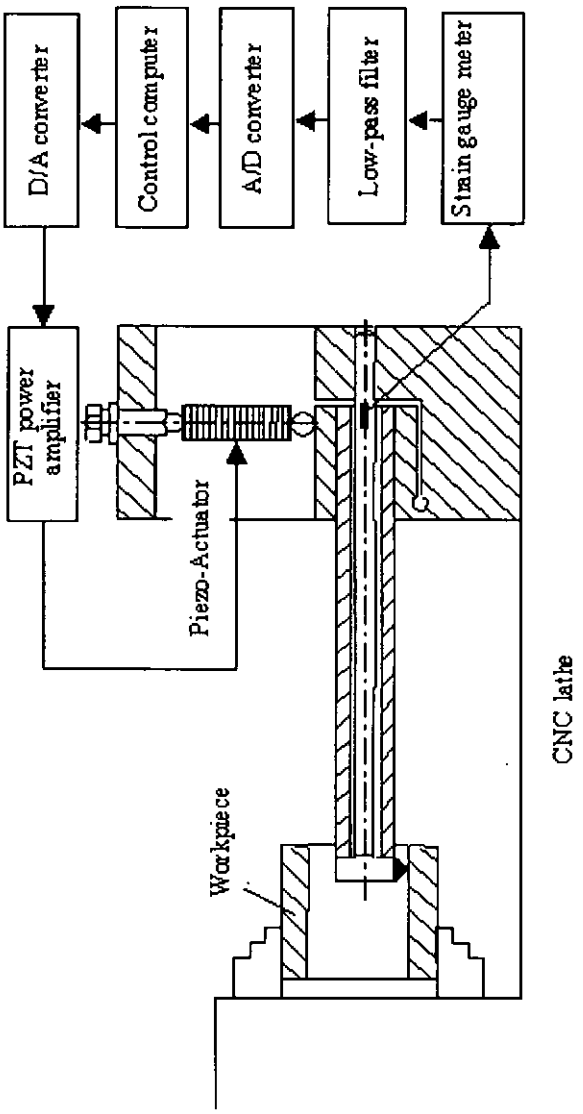

Fig. 3.2 The schematic arrangement of the experimental setup

The main steps in operating the proposed micro-boring servo system are as follows:

(1) the deflection of the micro-boring bar from the present position in the boring operation is measured as an in-process error by the two strain gauges attached to the measuring bar;

(2) the analog error signal is transformed to digital format through an A/D converter for data logging;

(3) the sampled data is processed in the personal computer;

(4) the digital output control command is transformed back to an analog signal through the D/A converter and sent to the piezo-actuator power amplifier; and

(5) the deflection of the boring bar is suppressed through the compensatory action of the piezoelectric actuator, resulting in improved machining accuracy.

As shown in Fig. 3.3, when the cutting force F =0, the control bar and measuring bar both remain level (Fig. 3.3a). When the control bar is deflected downwards as the cutting force, F > 0, acts on it, the measuring bar is also deflected downwards (Fig. 3.3b) and the error signal measured by the strain gauge meter increases. This error signal is input to the computer through the A/D converter and compared with the expected value. The piezoelectric actuator then expands by increasing the applied voltage to the PZT power amplifier through the D/A interface. As a result, the control bar rotates around the flexural hinge in clockwise direction, and the downward deflection of the cutter is suppressed, and the measuring bar becomes level again even if the control bar is bent more (Fig.

3.3c). On the other hand, when the boring cutter deflects upward as the cutting force is reduced, the deflection is then compensated by decreasing the applied voltage to the piezoelectric actuator. Hence, the deflection of the boring cutter can be compensated by the computer-controlled piezoelectric actuator system and the resulting accuracy be improved.

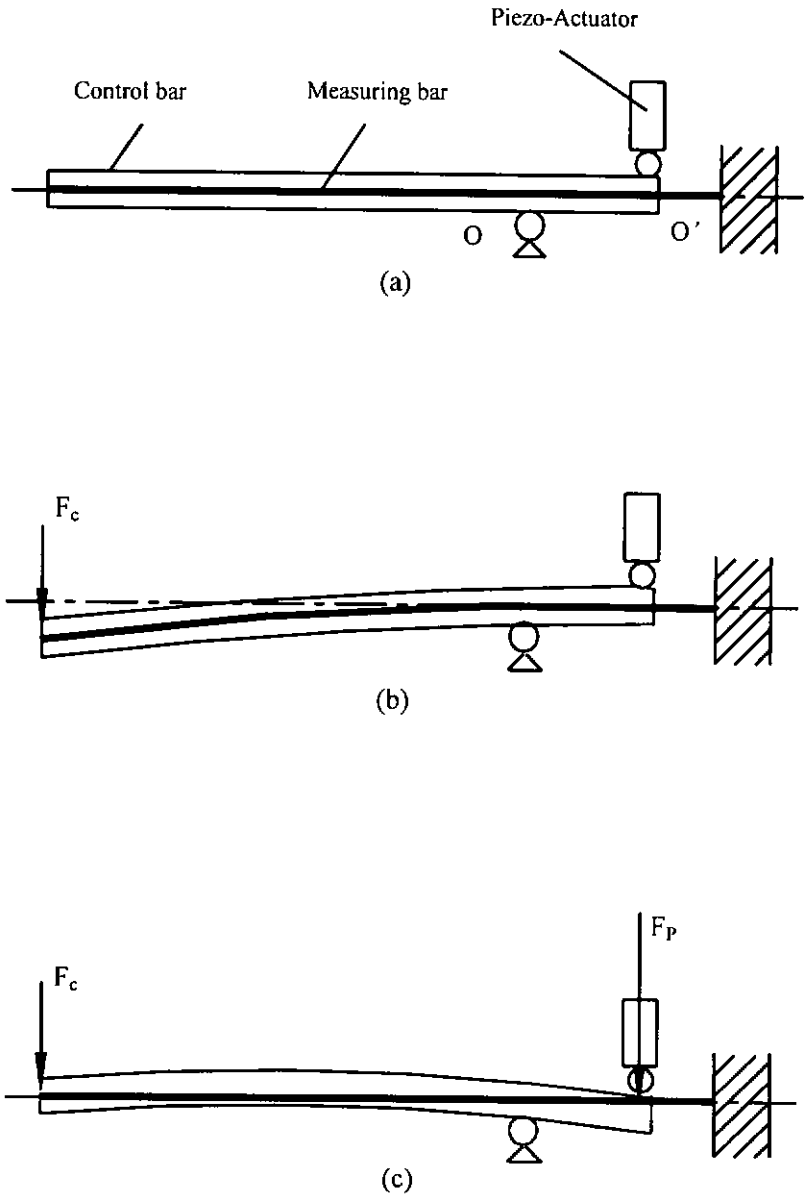

Fig.3.3 The deflection of the boring bar in error compensation operation

3.2 Mechanical Design

The boring bar is composed of a control bar and a measuring bar. The control bar is in a lever structure with a flexural pivot, while the measuring bar is in a cantilever structure. This section will deal with the design of the two bars respectively.

3.2.1 Control bar

A schematic diagram of the control bar is shown in Fig. 3.4. The control bar is made from a block of stainless steel through EDM wire-cut machining. The control bar is made into a lever structure with a flexural hinge as its fulcrum. The piezoelectric actuator and boring cutter are positioned in the two ends of the control bar respectively. The piezoelectric actuator drives the control bar to rotate about the flexural fulcrum as the voltage to the piezoelectric actuator changes. As a result, the deflection error of the boring cutter is compensated. In the design of the control bar, two factors considered are resonance of the boring bar and force magnitude with respect to the micro-feeding of the piezoelectric actuator. Higher stiffness means higher resonance frequency. However, more force is also required to move the boring cutter and the load capability of the actuator is very critical.

1. Design Consideration

The design structure of the flexural fulcrum is shown in Fig. 3.5. The angle stiffness of the flexural fulcrum can be derived as [Par65]:

$$K_\theta = \frac{4Ebt^{5/2}}{9\pi\rho^{1/2}} \qquad (3\text{–}1)$$

Where b— the width of the flexural fulcrum

ρ— the radius of curvature

t— minimum thickness of the flexural fulcrum

E—Young's modules of the material

Under the cutting force, the deflection of the boring cutter includes two parts, one part (Δ_1)caused by the anglular deflection of the flexural fulcrum, and the other(Δ_2) caused by the bending of the control bar.

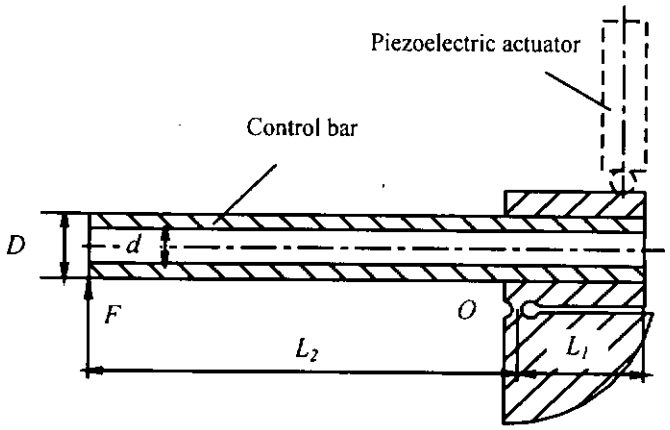

Fig. 3.4 The schematic diagram of the control bar

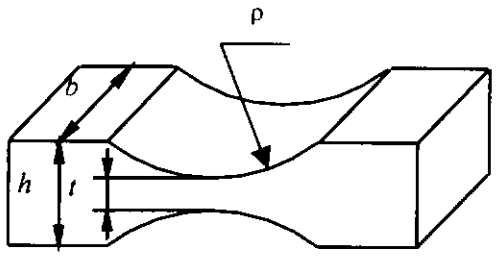

Fig.3.5 The structure of the flexural pivot

(1) the deflection caused by the angle deflection of the flexural fulcrum, Δ_1, can be obtained as:

$$\Delta_1 = L_2 \times \theta \ , \qquad \theta = \frac{M}{K_\theta} = \frac{FL_2}{K_\theta} \tag{3–2}$$

Where θ—the rotation angle of the flexural fulcrum

L_2 —the distance from the cutter to the flexural fulcrum

M —the moment acted on the flexural fulcrum

F — the cutting force

Substituting Eq. (3–1) into Eq. (3–2), we can obtain

$$\Delta_1 = \frac{FL_2^2}{K_\theta} = \frac{9FL_2^2\pi\rho^{1/2}}{4Ebt^{5/2}} \tag{3–3}$$

(2) the deflection caused by the bending of the control bar, Δ_2, can be obtained as:

$$\Delta_2 = \frac{FL_2^3}{3EI} \ , \qquad I = \frac{\pi}{64}(D^4 - d^4) \tag{3–4}$$

Where E — Young's modules of the material

I — the moment of inertia

(3) The overall stiffness of the control bar, K_c, can be obtained as:

$$K_c = \frac{F}{\Delta_1 + \Delta_2} \tag{3–5}$$

Substituting Eq. (3–3) and Eq. (3–4) into Eq. (3–5), we can obtain

$$K_c = \frac{3EIK_\theta}{L_2^2(3EI + L_2K_\theta)} \tag{3–6}$$

2. Interaction of the control bar

The sketch map of the interaction motion of the control bar is shown in Fig.3.6. Because the axes of the control bar is at an angle α to the line linking the boring cutter and the flexural pivot, the boring cutter will move not only in the radial direction but also by a small amount in the axial direction, when the piezoelectric actuator elongates. The relationship between the motion in axial direction, S_a, and that in radial direction, S_r, is as:

(a) In the case of the boring cutter locating at point A

$$\frac{S_a}{S_r} = tg\alpha_1 = \frac{\delta}{L_2} \tag{3–7}$$

(b) In the case of the boring cutter locating at point B

$$\frac{S_a}{S_r} = tg\alpha_2 = \frac{\delta + D}{L_2} \tag{3–8}$$

The motion interaction of the boring bar with cutter locating at point A is smaller than that at point B. In order to reduce the interaction between the motion of the boring cutter in axial and radial direction, the boring cutter is installed near point A. This installation also can protect the piezoelectric actuator from damage. If there is an accident force in the boring operation, the pulse force will push the boring bar to rotate clockwise and not act on the piezoelectric actuator.

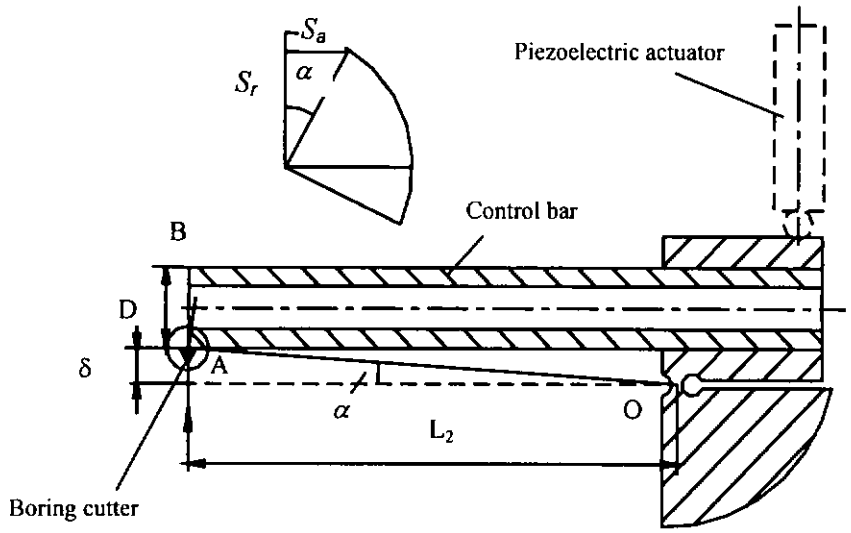

Fig.3.6 The motion error of the control bar

3.2.2 Measuring bar

In order to make the outer diameter of the boring bar smaller, strain gauges were employed to measure the deflection of the boring cutter indirectly. The measuring bar is made into a cantilever structure with two strain gauges attached to the root end, and the free end is joined with the cutter and control bar. The schematic diagram of the measuring bar is shown in Fig.3.7. When the cutter deflects Δ,The force, F_m, acting on the measuring bar at the cutter point is

$$F_m = \frac{3EI}{L_0^3}\Delta \ , \qquad I = \frac{\pi}{64}d_0^4 \tag{3–9}$$

Where d_0 — the diameter of the measuring bar

L_0 — the length of the measuring bar

E — Young's modules of the material

I — the moment of inertia

The strain near the root end of the measuring bar, ε, can be obtained as

$$\varepsilon = \frac{d_0}{2} \bullet \frac{F_m L_0}{EI} \tag{3–10}$$

Substituting Eq. (3–9) into Eq. (3–10), we can obtain

$$\varepsilon = \frac{3d_0}{2L_0^2}\Delta \tag{3–11}$$

From Eq. (3–11), we can see that ε is proportional with Δ, so the micro-feed of the boring cutter can be measured by the strain gauge.

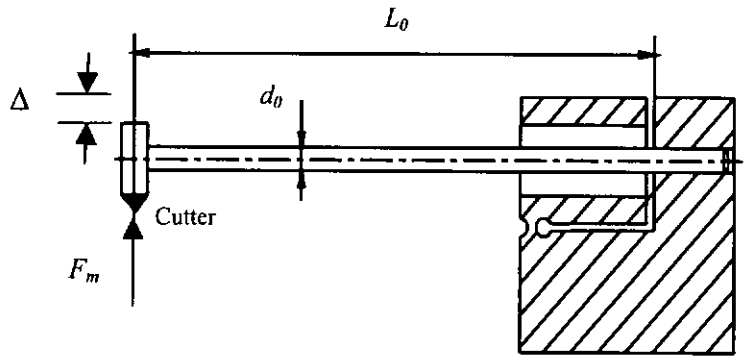

Fig. 3.7 Structure of the measuring bar

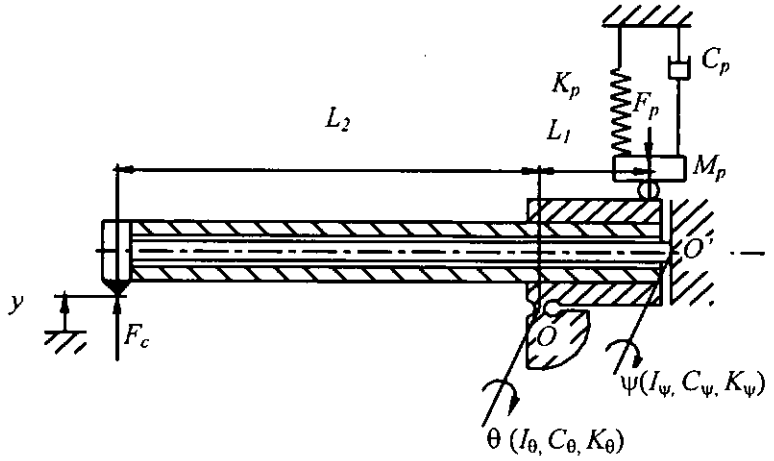

Fig. 3.8 Dynamic model for the boring bar

3.2.3 Motion model of boring bar

The dynamic equation describing the boring bar servo system is very useful in understanding its behavior. The model for the boring bar servo is shown in Fig. 3.8. For this purpose, the piezoelectric actuator is considered as a single degree of freedom system with lumped mass, stiffness and viscous dissipation elements denoted as M_p, K_p, and C_p respectively. In Fig. 3.8, y stands for the radial deflection of the cutter, Δ for the expansion of the piezoelectric actuator. θ stands for the angular position of the control bar about point O, ψ, angle of rotation, for the measuring bar about point O'. I_θ stands for the moment of inertia of the control bar about the axis of rotation (point O), I_ψ for the measuring bar about the axis of rotation (point O'). C_θ, K_θ are the viscous dissipation and stiffness of the control bar (about point O) and C_ψ, K_ψ for measuring bar (about point O'). F_c and F_p stand for the radial cutting force and the compensation force from piezoelectric actuator respectively. Assuming that the angle ψ and θ can be simplified as equal variables for small departures from the equilibrium position, the dynamic equation describing this boring bar servo can be obtained as

$$M\,\ddot{y} + C\,\dot{y} + K\,y = F_c + \frac{L_1}{L_2}F_p \qquad (3\text{–}12)$$

Where

$$M = (I_\theta + I_\psi + L_1^2 M_p)/L_2^2$$
$$C = (C_\theta + C_\psi + L_1^2 C_p)/L_2^2$$
$$K = (K_\theta + K_\psi + L_1^2 K_p)/L_2^2$$

Two useful equations for the design of the boring bar servo can be obtained from equation (3–12). The first equation determines the maximum unconstrained radial tool travel, y_{max}, which can be expressed as equation (3–13), where Δ_{max} is the maximum unconstrained expansion for the piezoelectric actuator. And the second equation expressing the natural frequency of the micro-boring system ω_n, can be obtained as equation (3–14)

$$y_{\max} = \frac{L_1 L_2 K_p}{K_\theta + K_\psi + L_1^2 K_p} \Delta_{\max} \tag{3–13}$$

$$\omega_n = \sqrt{\frac{K_\theta + K_\psi + L_1^2 K_p}{I_\theta + I_\psi + L_1^2 M_p}} \tag{3–14}$$

3.2.4 Performances of boring bar

1. Stiffness

Fig. 3.9 shows the relationship between the force and the deflection of the boring bar caused by the force. It was found that the stiffness of the boring bar is about 2.7N/ μm .

2. Resonant frequency

The resonant frequency of the boring bar was tested by the hammer method. An impulsive force was applied to the boring bar near the cutter point, and the vibration of the boring bar caused by the pulse force was measured by a digital oscilloscope. The experimental result is shown in Fig.3.10, the above curve is the response in time domain, and the one below is the frequency domain. It was found that the resonant frequency of the boring bar is about 440Hz.

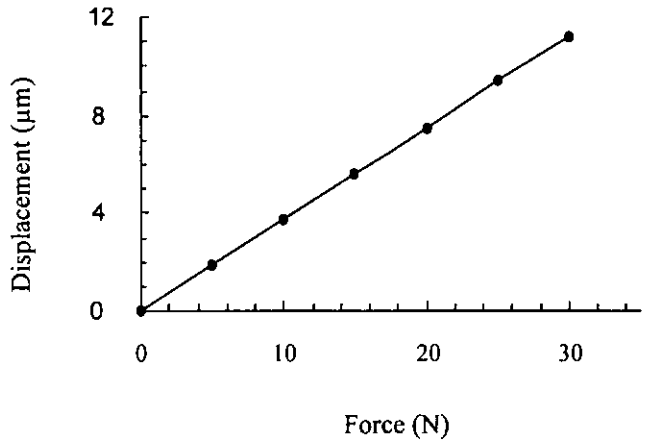

Fig.3.9 The static performance of the micro-boring bar

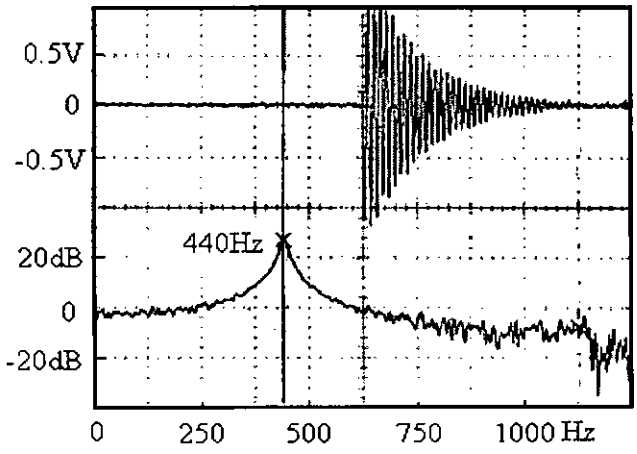

Fig. 3.10 The resonant frequency of the boring bar

3.3 Electronic Design

In this section, the selection of a position sensor along with a sampling card and a low pass filter for monitoring the tool tip displacement is discussed. Requirements and specifications for the small displacement actuator as well as the selection of the power amplifier are discussed. The experimental performances of the boring bar system are also described.

3.3.1 In-process measuring system

In this study, the position of the tool tip is detected by the strain gauge measuring system. The signal of the displacement of the boring cutter is sampled through a data acquisition card to the control computer.

3.3.1.1 PCL-818 data acquisition card

The PCL-818 Data Acquisition Card produced by the Advantech Co., Ltd. is used as a Analog-to-Digital Converter (ADC) to measure and convert the analog measurement values into 12 bit binary numbers, and it can also be used as a Digital-to-Analog Converter (DAC) to provide a means of changing the digital data into analog voltage in the boring bar operation. The specification of the PCL-818 Data Acquisition Card are summarized as follows:

1. A/D converter

- Channel: 16 single ended or 8 differential, switch selectable
- Resolution: 12 bits

- Input range: Unipolar: +10V, +5V, +2V, +1V

  Bipolar: ±10V, ±5V, ±2.5V, ±1V, ±0.5V
- Over-voltage: Continuous ±30V max
- Conversion type: Successive approximation
- Conversion speed: 100KHz max
- Accuracy: ±1bit(0.01% of reading)
- Linearity: ±1bit

2. D/A converter

- Channel: 2 channels
- Resolution: 12 bits
- Ouput range: 0 to +5V (+10V) with on-board -5V(-10V) reference,

  ±10V max. With external DC or AC reference.
- Reference: Internal -5V, -10V, or external DC or AC,±10V max
- Conversion type: 12 bit monolithic multiplying
- Linearity: ±0.5bit
- Output drive: ±5mA max

3.3.1.2 Boring bar deflection sensing system

The boring bar deflection sensing system consists of two precision strain gauges, a strain indicator and an operation amplifier noise filter. The two strain gauges are bonded to the measuring bar as shown in Fig.3.2. The strain gauges are connected into the adjacent arms of a Wheatstone bridge circuit in the TML Dynamic Strain Meter (Model DC-92D) which is used to measure and transform

the strains into an analog voltage (0–2.5V). The analog output of the indicator allows the computer to read through an A/D converter.

However, an operation amplifier noise filter is added in the path between the strain gauge meter and the computer because the output signal voltage from the strain gauge meter was so low that it was easily interfered by the environmental disturbance. The operational amplifier acted as a low pass filter as well as an amplifier of the strain gauge output signals.

1. Operation amplifier noise filter

In order to obtain a high quality signal of the deflection of the boring bar, an operation amplifier noise filter was employed to amplify the signal and filter the noise from the strain gauge meter. The circuit of the low-pass filter and amplifier is shown in Fig.3.11.

The amplifier parameter K can be obtained as

$$K = -\frac{R_2}{R_1} \tag{3–15}$$

Where: R_1 and R_2 are resistance

Let: $R_1 = 10K\Omega$, $R_2 = 75K\Omega$, we can obtain

$$K = -7.5$$

The cut-off frequency of the filter is

$$f_c = \frac{1}{2\pi RC} \tag{3–16}$$

Where R — value of the resistance

C — value of the capacitance

Let $C = 0.01\mu F$, $R = 130K\Omega$, we can obtain

$$f_c = \frac{1}{2\pi \times 130 \times 10^3 \times 0.01 \times 10^{-6}} = 120(Hz)$$

2. Principle of the strain gauge measurement

The strain gauges used in this study belonged to a general purpose family of strain gauges (model CEA–06–187UW–120, Measurement Group, Inc., U.S.A). They are connected into the adjacent arms of a Wheatstone bridge circuit as shown in Fig. 3.12. Where, R_1 and R_3 stand for two strain gauges, and R_2 and R_4 stand for regulative resistance. The symmetrically distributing position of the two strain gauges can counteract the noise caused by the environment.

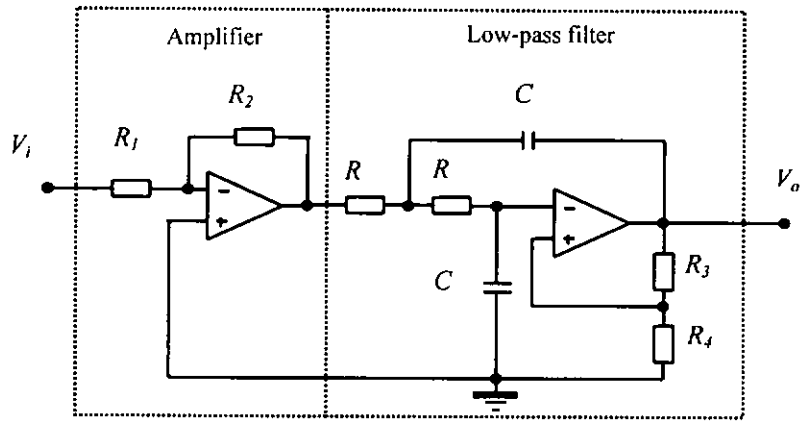

Fig.3.11 The circuit of low-pass filter and amplifier

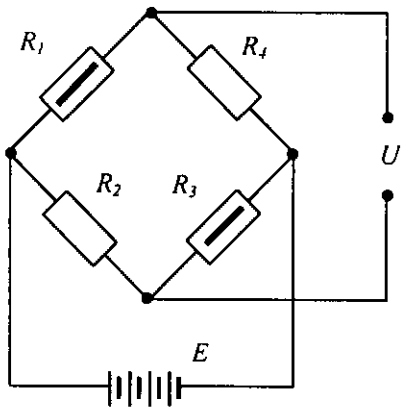

Fig.3.12 The schematic diagram of stain gauge Wheatstone bridge

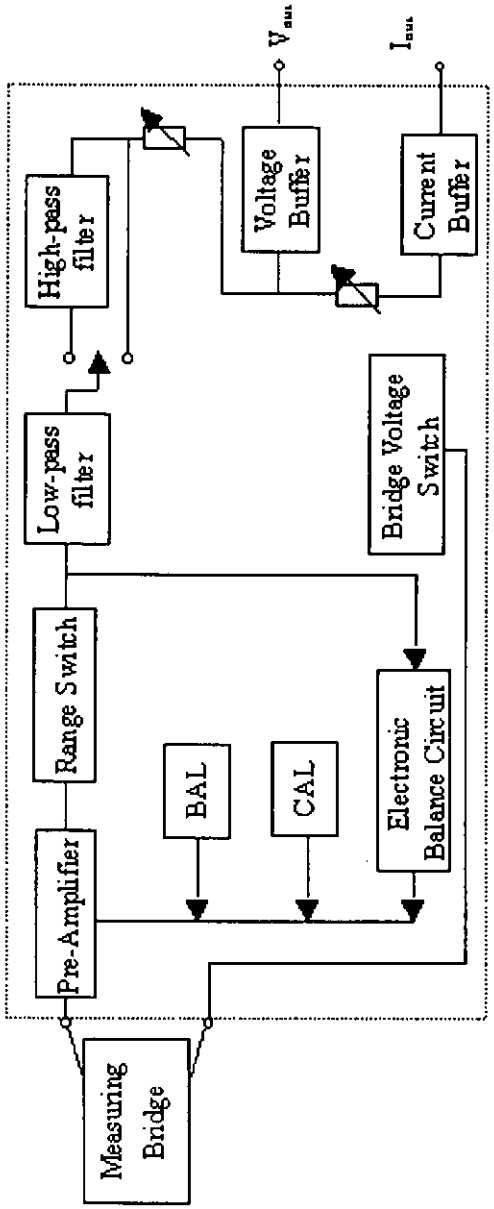

Fig.3.13 The block diagram of the principle of Strain Gauge Meter

The signal from the strain gauge bridge, U, can be calculated by the following equation

$$U = \frac{E}{4}\left[\frac{\Delta R_1}{R_1} - \frac{\Delta R_2}{R_2} + \frac{\Delta R_3}{R_3} - \frac{\Delta R_4}{R_4}\right] \tag{3–17}$$

Where E — the input voltage

Since the values of R_2, R_4 are constant, $\Delta R_2=\Delta R_4=0$, consider $R_1=R_3=R$, $\Delta R_1=\Delta R_3=\Delta R$, we can obtain

$$U = \frac{E}{4}\left[\frac{\Delta R_1}{R_1} + \frac{\Delta R_3}{R_3}\right] = \frac{E \cdot \Delta R}{2R} \tag{3–18}$$

Because $\frac{\Delta R}{R} = K_s\varepsilon$, we can obtain

$$U = \frac{E}{2}K_s\varepsilon \tag{3–19}$$

Where K_s — the ratio of strain

ε— the strain

Substituting Eq. (3–19) into Eq. (3–11), we can obtain

$$U = \frac{3d_0EK_s\Delta}{4L_0^2} \tag{3–20}$$

From Eq. (3–20), we can know that the signal from the strain gauge meter, U, is proportioned with the displacement of the cutter tip, Δ. It means that the deflection of the boring cutter can be effectively on-line measured by the strain gauge meter.

3. Strain gauge meter

The Dynamic Strain Meter (Model DC-92D) is used in this study (see Fig. 3.13). TML model DC–92D is a one channel DC exciting dynamic strain meter. Unlike the AC method, capacity balancing is not required. Moreover, an automatic electronic balancer is installed and initial balancing is achieved by simply pushing the button. The unit incorporates a low pass and high pass filter to eliminate higher harmonic or very low frequency unnecessary for measurement.

4. Calibration of the measuring system

In order to ensure that the strain gauge on-line measuring system can perform its function effectively, the measuring system was calibrated by the laser displacement meter (model KEYENCE LC 2 4 00A, Taylor Hobson Ltd.) with a high resolution of 0.02 μm and large measuring range of 100 μm. The block diagram of the strain gauge meter calibration system is shown in Fig.3.14. When the voltage is applied to the piezoelectric actuator, the displacement of the boring cutter was measured by the strain gauge meter and the laser meter respectively. The measurement results are shown in Fig. 3.15, where it is indicated that the strain gauge meter has good linearity.

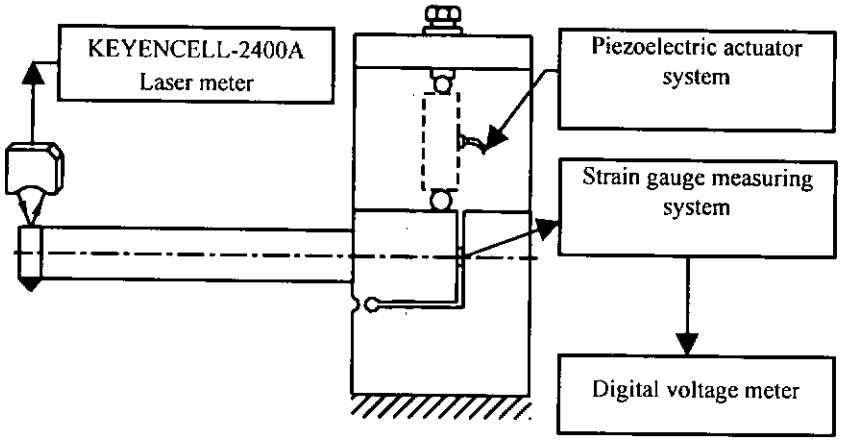

Fig.3.14 The block diagram of the strain gauge meter calibration system

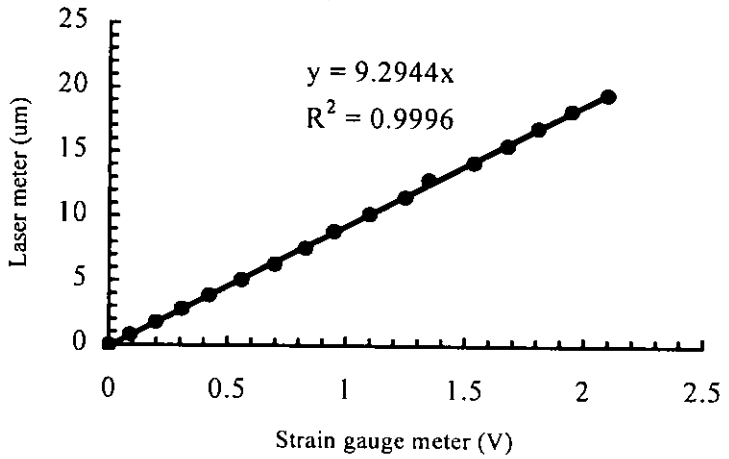

Fig.3.15 The calibration curve of the strain gauge meter

3.3.2 Actuator system

Most systems use rotating motors to produce motion. In many cases, linear motion is required. So it is necessary to convert from rotational to linear motion with the aid of mechanical components. However, this limits the accuracy that can be attained.

3.3.2.1 Piezoelectric actuator

The piezoelectric actuator is selected for assessing the movement and positioning of the boring cutter. It is made of stacked ceramic discs with a piezoelectric property. When a voltage is applied, the electric fields point in the direction of polarization which leads to an enlargement of the disc's thickness and therefore to an expansion of the stack.

Hysteresis is a common behavior between the applied voltage and the expansion of the piezoelectric materials. The same operating voltage can give different expansions depending on whether the actuator had previously received no applied voltage or the maximum applied voltage. The size of the hysteresis depends on the amplitude of the voltage change.

Usually the internal resistance of the piezoelectric actuator is more than 10M ohms. Hence the current through the ceramic, even with maximum operating voltage, can be neglected. In quasi-static operation, it can be treated as a simple capacitor. Once a charge actuator is separated from the power supply, its charge and expansion can be maintained for a period of time, until the charge is

dissipated through the internal resistance.

The expansion of the actuator depends on the number of the piled-up discs, the applied voltage, the piezoelectric constant and the force acting on it. Its resolution is theoretically unlimited, and depends merely on the stability of the applied voltage. The charge of the voltage is directly converted into a linear movement without any significant losses. The principle of a piezoelectric actuator is shown in Fig.3.16. The theoretical expansion of the piezoelectric actuator can be expressed as follows:

$$\delta(t) = N \times \gamma \times V(t) \tag{3–21}$$

Where $\delta(t)$ — the theoretical expansion of the actuator

N — the number of the piled-up discs

γ — the piezoelectric constant

$V(t)$ — the applied voltage

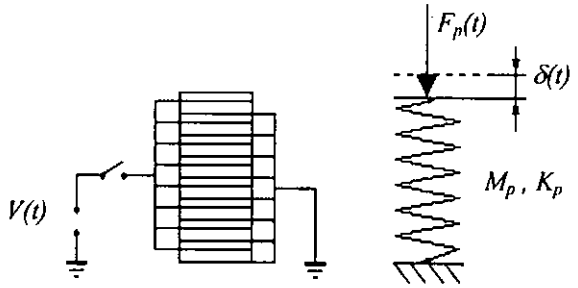

Fig. 3.16 The principle of piezoelectric actuator

Usually the practical expansion of the piezoelectric actuator is smaller than the theoretical expansion because of the force acting on it. The piezoelectric actuator can be considered as a system with mass, M_p , and stiffness, K_p (See Fig. 3.16). The practical expansion of the piezoelectric actuator is expressed as follows.

$$\Delta(t) = \delta(t) - \frac{F_p(t)}{k_p} \tag{3–22}$$

Where $F_p(t)$ — the force acted on the piezoelectric actuator

$\Delta(t)$ — the practical expansion of the piezoelectric actuator

Substituting Eq. (3–21) into Eq. (3–22), we can obtain

$$\Delta(t) = N\gamma V(t) - \frac{F_p(t)}{k_p} \tag{3–23}$$

LVPZ (low-voltage piezo) piezo-actuator is different from the traditional piezo-actuators because of the smaller applied voltage. The piezo effect is linearly dependent on the applied electric field. The high-voltage piezo-actuators are

generally operated with voltages of 1000V to 2000V, which means field strengths of up to 2000V/mm. By reducing the layer thickness a similar field strength can also be attained with a voltage of 100V. This is how the LVPZ operates. The distance between the electrodes has been reduced, thus reducing the required voltage. The field strength is about the same. This means that the LVPZ provides the same expansion per unit length as the traditional piezo-actuators. The capacity of the elements increase by the square and so the required charging current is much higher. The required electrical energy and power, however, remain approximately the same. The LVPZ have the advantage that both their stiffness per cross-sectional area and length are greater than those of high-voltage piezo-actuators and so their resonant frequency is higher. The LVPZ piezo-actuator in the model P–845.10 made by the Physik Instrument Co. is chosen for the boring bar system and its features are given as follows:

Nominal expansion at +100V:	15 μm
Maximum pushing force:	3000N
Maximum pulling force:	700N
Electric capacitance:	7 μF
Stiffness:	200N/ μm
Resonant frequency:	16KHz

3.3.2.2 Power amplifier

The dynamic driving capability of the piezoelectric actuator is determined by its capacitance impedance. The alternating current to be supplied to the actuator can be calculated by the following formula

$$i = 2\pi fCV \tag{3–24}$$

Where i — alternating current

f — current frequency

C — capacitance

V — applied voltage

A power amplifier E-863.10 made by the Phyick Instrument Co. is adopted for the piezoelectric actuator. The specifications of the power amplifier is as follows:

Output voltage range:	-20 to + 120 V
Maximum average output current:	60mA
Maximum output current:	140mA
Maximum Average power:	6 W (sinus)
Control signal:	-2 to +12V
Input impedance:	>100Kohm
Noise:	<15mVpp

The frequency response of the power amplifier is shown in Fig.3.17. The frequency response of the power amplifier is 3KHz when it is open, and 260Hz when open.

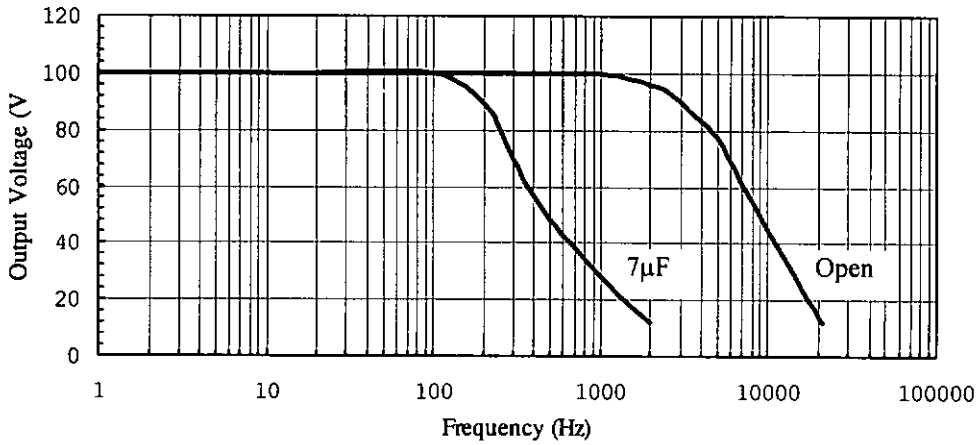

Fig. 3.17 The frequency response of the piezoelectric actuator power amplifier

3.3.3 Experimental analysis on compensating system

1. The relationship between applied voltage and expansion

The relationship between the expansion of the boring cutter and the control voltage applied to the piezo-actuator power amplifier is shown in Fig.3.18. The maximum expansion of the boring cutter is more than $20\,\mu m$. Due to the performance of the piezoelectric materials, there is hysteresis between the applied voltage and the expansion, which can be compensated by the program.

2. Resolution

The resolution of micro-boring system is shown in Fig.3.19. The resolution of the boring system is about $0.08\,\mu m$.

3. Frequency response of boring bar system

A sweep sine-wave signal is input to control the piezoelectric actuator, and the boring cutter move in a sine-wave way. The response of the boring cutter is shown in Fig.3.20. The above part is for time domain and the below part is for frequency domain analyzed by FFT method. It is indicated that the frequency response of the boring bar system is about 80 Hz.

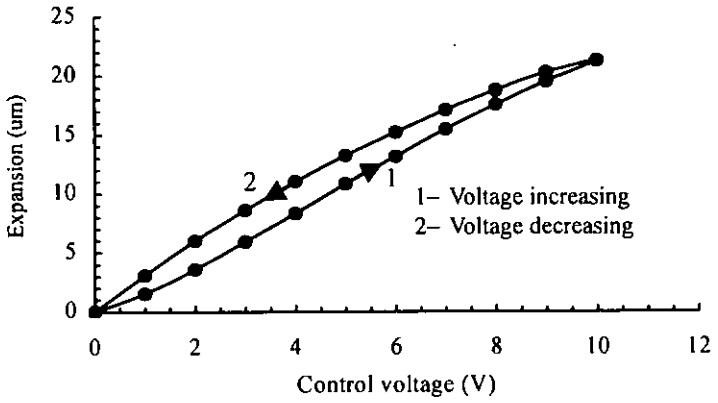

Fig.3.18 The static performance of the micro-feed system

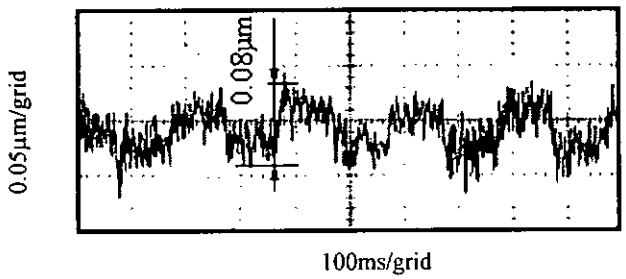

Fig.3.19 The resolution of micro-boring system

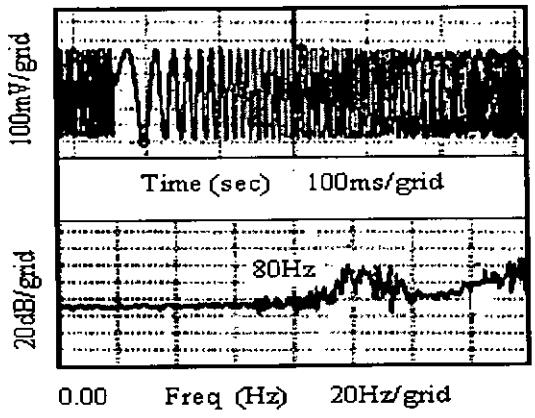

Fig.3.20 The frequency response of micro-boring bar system

Chapter Four

MODELING AND FORECASTING

A sequence of observed data usually ordered in time is called a time series, although time may be replaced by other variables such as space. The statistical methodology dealing with the analysis of such data is called Time Series Analysis. Two important aims of time series analysis are modeling and forecasting.

In the thesis work, Time Series Analysis is employed to study the machining errors of the boring operation. The deflection errors of the boring cutter at the cutting point are considered to be a stochastic process. In this study, the modeling of the errors is based on the Dynamic Data System (DDS) methodology. It uses dynamic data from the system response and/or input in the form of a time/space series to develop physically meaningful stochastic differences or differential equations. These stochastic equations can be utilized valuably in identifying the essential characteristics of the system through physical interpretations of the model parameters for system identification. They can also be used for control purposes since they give forecasts of the future values of the signal, which are optimized in the sense of minimum mean squared errors.

At first, the model structure of the time series such as the Autoregressive Moving Average (ARMA) model, Autoregressive (AR) model and Moving

Average (MA) model are introduced in Section 4.1. Then, the modeling technique and the criterion to determine the adequate order of the model are discussed in Section 4.2. Recursive model parameter estimation, which is a potential approach for on-line control modeling, is discussed in Section 4.3. Finally, Forecasting algorithms are presented in Section 4.4.

4.1 Model Structure

4.1.1 ARMA model

ARMA model is the basic and widest used model in the Time Series Analysis methodology. A stationary signal can be represented in discrete time by a stochastic difference equation of the form

$$\begin{aligned} x_t &= \phi_1 x_{t-1} + \phi_2 x_{t-2} + \cdots\cdots + \phi_n x_{t-n} \\ &\quad - \theta_1 a_{t-1} - \theta_2 a_{t-2} - \cdots\cdots - \theta_m a_{t-m} + a_t, \qquad a_t \sim NID(0, \sigma_a^2) \end{aligned} \tag{4–1}$$

or:

$$x_t = \sum_{i=1}^{n} \phi_i x_{t-i} - \sum_{j=1}^{m} \theta_j a_{t-j} + a_t \quad , \quad a_t \sim NID(0, \sigma_a^2) \tag{4–2}$$

where, ϕ_i (i=1, 2,……, n) are the autoregressive parameters

θ_j (j=1, 2, ……, m) are the moving average parameters

a_t is discrete white noise

The above equation shows that the present observation x_t is correlated with the past observations x_{t-i} at i=1, 2, …… , n and the random shocks a_t at t, t-1, …, t-m. From another point of view, the ARMA model shows how we can remove the dependence of a_t on x_{t-1}, x_{t-2},……, x_{t-n} and a_{t-1}, a_{t-2},……, a_{t-m} by the autoregressive

and moving average parts respectively.

This linear stochastic difference equation is commonly referred to as a discrete Auto-Regressive Moving-Average model of the n-th autoregressive order and the m-th moving average order. It is denoted by an ARMA (n, m) model.

4.1.2 Special cases of ARMA model

In the ARMA model, if θ_j (j=1, 2, ..., m)=0, we can obtain a linear AR model as in Eq.(4–3)

$$x_t = \sum_{i=1}^{n} \phi_i x_{t-i} + a_t, \qquad a_t \sim NID(0, \sigma_a^2) \tag{4–3}$$

Theoretically speaking, the ARMA model structure can be equivalently represented by the AR model with an order of infinity. In practice, a finite AR model is often used to approximate the infinity model.

Another special case of the ARMA model is MA model which is obtained in the case that ϕ_i (i=1, 2,....., n)=0. MA model is written as:

$$x_t = a_t - \sum_{j=1}^{m} \theta_j a_{t-j}\ , \qquad a_t \sim NID(0, \sigma_a^2) \tag{4–4}$$

4.2 Model Building

The parameter estimation of AR(n) or ARMA(n, m) is based on the same criterion, which minimizes the sum of square of residuals. However, ARMA modeling requires a nonlinear least-squares estimation procedure because the unconditional regression is nonlinear. The nonlinear least-squares estimation

procedure not only leads to a relatively long computing time but also is difficult to implement on a micro-computer which is used for on-line modeling and control.

On the other hand, the parameter of the AR model can be estimated by the linear least-squares method. Therefore, AR modeling is sometimes much more convenient and efficient to implement on a microcomputer both in terms of software and computation time. Based on Eq. (4–3), we can obtain:

$$\begin{cases} x_{n+1} = \phi_1 x_n + \phi_2 x_{n-1} + \cdots\cdots + \phi_n x_1 + a_{n+1} \\ x_{n+2} = \phi_1 x_{n+1} + \phi_2 x_n + \cdots\cdots + \phi_n x_2 + a_{n+2} \\ \cdots\cdots \\ x_N = \phi_1 x_{N-1} + \phi_2 x_{N-2} + \cdots\cdots + \phi_n x_{N-n} + a_N \end{cases} \tag{4–5}$$

Eq. (4–5) can be expressed in matrix form as following

$$[Y] = [X][\phi] + [a] \tag{4–6}$$

where,

$$[Y] = [x_{n+1} \quad x_{n+2} \cdots\cdots \quad x_N]^T$$

$$[\phi] = [\phi_1 \quad \phi_2 \cdots\cdots \quad \phi_n]^T$$

$$[a] = [a_{n+1} \quad a_{n+2} \cdots\cdots \quad a_N]^T$$

$$[X] = \begin{bmatrix} x_n & x_{n-1} & \cdots\cdots & x_1 \\ x_{n+1} & x_n & \cdots\cdots & x_2 \\ \cdots\cdots & & & \\ x_{N-1} & x_{N-2} & \cdots\cdots & x_{N-n} \end{bmatrix}$$

By use of the least-squares estimation, the autoregressive parameters can be

obtained as follows [Pan83].

$$[\phi] = \left([X]^T[X]\right)^{-1}[X]^T[Y] \tag{4–7}$$

where, $[\cdot]^T$ stand for matrix transpose, $[\cdot]^{-1}$ stand for matrix inversion

The unanswered question is how to decide the adequate order of the model. Basically, there are three criteria for checking the adequacy of the model; the Q-test, the F-test, and the AIC test. Among these three methods, AIC (Akaike's Information Criterion) is commonly used. For an AR(n) model, the AIC is defined as

$$AIC(r) = N \ln[\sigma_a^2 /(N - r)] + 2r$$

where

σ_a^2: the residual sum of squares

r : the total number of parameters including the mean, i. e., r=n+1

N: the number of observations

Typically, the value of AIC decreases quickly as the number of parameters being adjusted is decreased, then, it increases almost linearly when too many redundant parameters are included. The set of parameters which produce a minimum AIC value is chosen as the adequate model.

4.3 Recursive Model Parameter Estimation

The modeling technique discussed in Section 4.2 is a batch modeling method, which generally needs a longer computing time. In the batch modeling method, all

sampled data are used in each parameter calculating operation. The recursive modeling technique estimates the model parameters after each sampled data, and is faster than the batch modeling. Therefore, this modeling method is used in on-line modeling for a time variant system or non-stationary signal.

Many recursive parameter estimation methods have been developed, several comparison studies can be found in the literature [Gro80, Ise74, Sar76] Among these methods, there is a strong similarity in the algorithm of the form

$$[\phi]_{t+1} = [\phi]_t + [M]e \tag{4–8}$$

Where,

$[\phi]_t$: parameter matrix at angle t

$[M]$: the correcting vector

e: the forecasting error

One of the most basic and commonly employed recursive parameter estimation methods is the Recursive Least Square (RLS) method. In many problems of real-time identification, the matrix $[X]$ in equation (4–7) is successively updated by new measurement data. It is uneconomical to repeat the calculation of parameters with all past measured data stored in the matrix $[X]$. When the parameters are estimated by the least-squares technique from the data, an economic and powerful recursive method can be used to reduce the number of numerical operations.

For an AR model of order n of equation (4–3) at angle t=N, let the parameter vector

$$[\phi]_t = [\phi_1 \quad \phi_2 \cdots\cdots \quad \phi_n]^T \tag{4–9}$$

and the data vector

$$[Z]_t = [x_{N-1} \quad x_{N-2} \cdots\cdots \quad x_{N-n}]^T \tag{4–10}$$

when an additional data X_{N+1} is obtained at angle t=N+1, the following notation will be used,

$$[Z]_{t+1} = [x_N \quad x_{N-1} \cdots\cdots x_{N-n+1}]^T \tag{4–11}$$

$$[Y]_{t+1} = [x_{n+1} \quad x_{n+2} \cdots\cdots x_{N+1}]^T = \begin{bmatrix} [Y]_t \\ x_{t+1} \end{bmatrix} \tag{4–12}$$

$$[X]_{t+1} = \begin{bmatrix} [X]_t \\ [Z]_{t+1}^T \end{bmatrix} \tag{4–13}$$

The least-square estimate of parameters is performed according to equation (4–7)

$$\begin{aligned} [\phi]_{t+1} &= \left([X]_{t+1}^T [X]_{t+1}\right)^{-1} [X]_{t+1}^T [Y]_{t+1} \\ &= \left([X]_t^T [X]_t + [Z]_{t+1}[Z]_{t+1}^T\right)^{-1} \left([X]_t^T [Y]_t + [Z]_{t+1} x_{t+1}\right) \end{aligned} \tag{4–14}$$

Using the "Matrix inversion lemma", the inverted matrix on the right-hand side of equation (4–14) is [Lee64]

$$\begin{aligned} &\left([X]_t^T [X]_t + [Z]_{t+1}[Z]_{t+1}^T\right)^{-1} \\ &= \left([X]_t^T [X]_t\right)^{-1} - \left([X]_t^T x_t\right)^{-1} [Z]_{t+1} \left(1 + [Z]_{t+1}^T \left([X]_t^T [X]_t\right)^{-1} [Z]_{t+1}\right)^{-1} \\ &\quad [Z]_{t+1}^T \left([X]_t^T [X]_t\right)^{-1} \end{aligned} \tag{4–15}$$

Now, by introducing a "correcting vector",

$$[M]_{t+1} = \left([X]_t^T x_t\right)^{-1} [Z]_{t+1} \left(1 + [Z]_{t+1}^T \left([X]_t^T [X]_t\right)^{-1} [Z]_{t+1}\right)^{-1} \tag{4–16}$$

Therefore,

$$[\phi]_{t+1} = \left(\left([X]_t^T[X]_t\right)^{-1} - [M]_{t+1}[Z]_{t+1}^T\left([X]_t^T[X]_t\right)^{-1}\right.$$
$$\left.\left([X]_t^T[Y]_t + [Z]_{t+1}x_{t+1}\right)\right.$$

$$[\phi]_{t+1} = [\phi]_t + [M]_{t+1}\left(x_{t+1} - [Z]_{t+1}^T[\phi]_t\right) \qquad (4\text{–}17)$$

It is evident that the updated estimated parameter corresponding to the t+1 sample is equal to the previous parameter corrected by the term $(x_{t+1}-[Z]^T_{t+1}[\phi]_t)$ and the correcting factor $[M]_{t+1}$. The product $[Z]^T_{t+1}[\phi]_t$ may be considered as the prediction of the value x based on model parameter $[\phi]_t$ and on the set of data $[Z]^T_{t+1}$.

In order to calculate the elements of matrix $[M]_{t+1}$, it is possible to introduce

$$[P]_{(t)} = \alpha\left([X]_t^T[X]_t\right)^{-1} \qquad (4\text{–}18)$$

where α is a positive constant and may be selected in the interval $0<\alpha\leq 1$.

Then

$$[M]_{t+1} = [P]_{(t)}[Z]_{t+1}\left(\alpha + [Z]_{t+1}^T[P]_{(t)}[Z]_{t+1}\right)^{-1} \qquad (4\text{–}19)$$

Substituting the matrix $[P]_{(t)}$ in equation (4–18) into equation (4–19), we can obtain

$$[P]_{(t+1)} = \left(I - [M]_{t+1}[Z]_{t+1}^T\right)[P]_{(t)} \qquad (4\text{–}20)$$

Therefore, the estimate of parameters according to the least-squares approach may be calculated by the recursive formulas equation (4–19), equation (4–16) and (4–17).

To start the recursive algorithm, one generally sets initial values

$$\phi(0) = 0, \qquad [P]_{(0)} = \beta I$$

With large. It is suggested that an estimate of a suitable is [Kim86]:

$$\beta = \frac{10 \times \sum_{i=0}^{N} x^2(i)}{N+1}$$

4.4 Forecasting of Machining Errors

4.4.1 Principle of forecasting

For a stationary stochastic system or time series, given the observations x_t, x_{t-1}, x_{t-2}, ..., at angle t, we can obtain by Word's decomposition [Kim86].

$$x_t = \sum_{j=0}^{\infty} G_j a_{t-j} \tag{4–21}$$

where G_j is the Green's function, and the a_t's are uncorrelated or orthogonal. Therefore,

$$x_{t+l} = \left(G_0 a_{t+l} + G_1 a_{t+l-1} + \cdots\cdots + G_{l-1} a_{t+1}\right) + \left(G_l a_t + G_{l+1} a_{t-1} + \cdots\cdots\right) \tag{4–22}$$

In equation (4–22), a_t ,a_{t-1}, a_{t-2} ,...,a_1 are known, and the part of $(G_l a_t + G_{l+1} a_{t-1} + \cdots\cdots)$ is decided, which is denoted as $\hat{x}_t(l)$. Since a_t's are white noise, we can not predict the values of a_{t+1}, a_{t+2}, ..., a_{t+l}. The part of $\left(G_0 a_{t+l} + G_1 a_{t+l-1} + \cdots\cdots + G_{l-1} a_{t+1}\right)$ is unknown, which is denoted as $e_t(l)$. Equation (4–22) can be rewritten as

$$x_{t+l} = e_t(l) + \hat{x}_t(l) \tag{4–23}$$

where, $\hat{x}_t(l)$ is the best linear l-step forehead prediction of x at angle t and $e_t(l)$ is

the prediction error. Equation (4–23) is the basic principle of forecasting. However, the Green's function is an infinite series, so using G for forecasting purposes is inconvenient. A simple method of computing the forecasts can be obtained by conditional expectation. If we take the conditional expectation at angle t, denoted by E, of both sides of equation (4–22), we have

$$\begin{aligned} E(x_{t+l}) &= E\left(G_0 a_{t+l} + G_1 a_{t+l-1} + \cdots\cdots + G_{l-1} a_{t+1}\right) + E\left(G_l a_t + G_{l+1} a_{t-1} + \cdots\cdots\right) \\ &= E\left(G_l a_t + G_{l+1} a_{t-1} + \cdots\cdots\right) \end{aligned} \tag{4–24}$$

Comparing equation (4–24), (4–22) and equation (4–23) we find

$$E(x_{t+1}) = \hat{x}_t(l) \tag{4–25}$$

4.4.2 AR model forecasting

Consider the AR(n) model

$$x_t = \phi_1 x_{t-1} + \phi_2 x_{t-2} + \cdots\cdots + \phi_n x_{t-n} + a_t, \qquad a_t \sim NID(0, \sigma_a^2) \tag{4–26}$$

According to equation (4–26), when l=1, the 1-step forehead forecasting of x is

$$\hat{x}_t(1) = E[x_{t+1}] = E\left[\phi_1 x_t + \phi_2 x_{t-1} + \cdots\cdots + \phi_n x_{t+1-n} + a_{t+1}\right] \tag{4–27}$$

At angle t, the value of $x_t, x_{t-1}, a_{t-2}, \ldots, x_{t+1-n}$ is known and a_{t+1} is not happened, so E[a_{t+1}]=0, and equation (4–27) can be written as

$$\hat{x}_t(1) = \phi_1 x_t + \phi_2 x_{t-1} + \cdots\cdots + \phi_n x_{t+1-n} \tag{4–28}$$

As the same, in the case of l=1, the 2-step forehead forecasting of x is

$$\begin{aligned}\hat{x}_t(2) = E[x_{t+2}] &= E[\phi_1 x_{t+1} + \phi_2 x_t + \cdots\cdots + \phi_n x_{t+2-n} + a_{t+2}] \\ &= \phi_1 E[x_{t+1}] + \phi_2 x_t + \cdots\cdots + \phi_n x_{t+2-n} \\ &= \phi_1 \hat{x}_t(1) + + \phi_2 x_t + \cdots\cdots + \phi_n x_{t+2-n}\end{aligned} \tag{4–29}$$

Obviously, the l-step forehead forecasting value of x is

$$\begin{aligned}\hat{x}_t(l) = \phi_1 \hat{x}_t(l-1) + \phi_2 \hat{x}_t(l-2) + \cdots\cdots + \phi_{l-1} \hat{x}_t(1) + \phi_l x_t \\ + \phi_{l+1} x_{t-1} + \cdots\cdots + \phi_n x_{t+l-n}\end{aligned} \quad (l \le n) \tag{4–30}$$

$$\hat{x}_t(l) = \phi_1 \hat{x}_t(l-1) + \phi_2 \hat{x}_t(l-2) + \cdots\cdots + \phi_n \hat{x}_t(l-n) \quad (l > n) \tag{4–31}$$

So the forecasting of the AR Model can be expressed as the following:

$$\hat{x}_t(l) = \begin{cases} \sum_{i=1}^{n} \phi_i x_{t+l-i} & (l = 1) \\ \sum_{i=1}^{l-1} \phi_i \hat{x}_t(l-i) + \sum_{i=l}^{n} \phi_i x_{t+l-i} & (1 < l \le n) \\ \sum_{i=1}^{n} \phi_i \hat{x}_t(l-i) & (l > n) \end{cases} \tag{4–32}$$

4.4.3 ARMA model forecasting

Consider the ARMA (n, m) model

$$x_{t+l} = \sum_{i=1}^{n} \phi_i x_{t+l-i} + \sum_{j=1}^{m} \theta_j a_{t+l-j} + a_{t+l} \tag{4–33}$$

Taking expectation of both side of equation (4–33)

$$E[x_{t+l}] = E\left[\left(\sum_{i=1}^{n}\phi_i x_{t+l-i} + \sum_{j=1}^{m}\theta_j a_{t+l-j}\right) + a_{t+l}\right] \tag{4–34}$$

Comparing equation (4–34) and equation (4–25), we can obtain

$$\hat{x}_t(l) = E\left[\left(\sum_{i=1}^{n}\phi_i x_{t+l-i} + \sum_{j=1}^{m}\theta_j a_{t+l-j}\right) + a_{t+l}\right] \tag{4–35}$$

Under the following rules of conditional expectation,

$$\begin{cases} E[x_{t-j}] = x_{t-j} & (j = 0, 1, 2, \cdots\cdots) \\ E[x_{t+j}] = \hat{x}_t(j) & (j = 1, 2, 3, \cdots\cdots) \\ E[a_{t-j}] = a_{t-j} & (j = 0, 1, 2, \cdots\cdots) \\ E[a_{t+j}] = 0 & (j = 1, 2, 3, \cdots\cdots) \end{cases} \tag{4–36}$$

We can obtain

$$\hat{x}_t(l) = \sum_{i=1}^{l-1}\phi_i \hat{x}_t(l-i) + \sum_{i=l}^{n}\phi_i x_{t+l-i} - \sum_{j=0}^{m-l}\theta_j a_{t+l-j} \tag{4–37}$$

Chapter Five

CONTROL ALGORITHM

In this chapter, a proposed approach for on-line machining errors control is presented based on investigated concepts of stochastic modeling, forecasting and minimum variance control in Chapter 4. A comprehensive control strategy, Forecasting Compensatory Control (FCC), for effective machining accuracy improvement is proposed in this chapter and the control program of the boring system is also introduced in this chapter.

5.1 Strategies for FCC

The FCC scheme, which is a proposed solution to the problems associated with the in-process measurement of machining accuracy, is based on obtaining an "error model" of the tool error measured in-process, then forecasting the error at the cutting point to compensate it with the appropriate compensatory action.

This approach is a combination of in-process gauging, modeling and active compensatory control. In this approach, there are two features of substantial importance: stochastic modeling and optimum forecasting. Through stochastic modeling, the tool errors are represented by a model of a simple structure in the form of the AR or ARMA model without the necessity of obtaining the complex cause-and-effect relationships between various errors and error sources. And more

importantly, it is possible to account for the random parts of the error as well as its repeatable parts. Optimum forecasting is an important prerequisite for a rational control strategy, considering the inevitable time delay associated with sensing, computing and actuation. This capability of forecasting can alleviate the problem associated with in-process measurement of machining errors, since the measurement delay can, for the most part, be compensated for by optimum forecasting.

The proposed FCC control system in this research has the structure of a feedback control system, with a special feature that the compensating signal is based on a forecast value rather than a measured value, which has some time delay. A block diagram of the overall FCC control structure is presented in Fig. 5.1. G_c is the transfer function of the control bar system. G_p is the transfer function of the piezoelectric actuator power amplifier. G_a is the transfer function of the piezoelectric actuator. G_f is the transfer function of the amplifier-filter. The disturbance represents the error sources affecting workpiece accuracy. The output is the deflection error of the boring cutter measured in-process.

The main steps of the proposed system operation for the cylindricity control are as follows:

Step 1: the deflection error in the boring operation is obtained in-process by a strain-gauge-based measurement system.

Step 2: the error data is reconstructed to get the real cutting error in the sensitive direction.

Step 3: this error is modeled to obtain the error model through the stochastic modeling technique.

Step 4: the deflection error at the cutting point is forecasted.

Step 5: finally, the forecasted error is corrected by the minimum variance control through the compensatory motion of the actuator system.

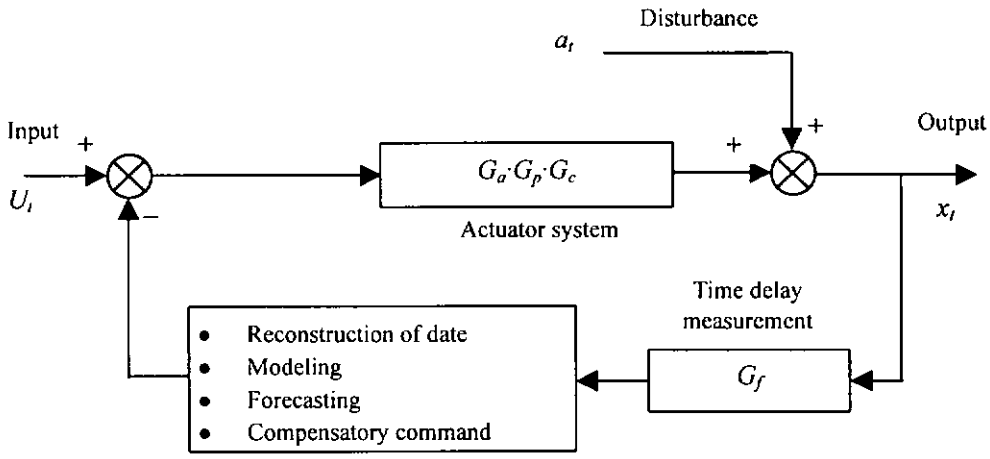

Fig. 5.1 The block diagram of the FCC controller

5.2 Transfer Function of Boring System

The dynamic mathematical model of the boring bar system is very useful for the analysis and the improvement of the closed-loop performance. The models usually are represented by the transfer function for a linear continuous system, or described by an infinite difference equation and the ARMA model for the discrete system.

There are three kinds of experimental identification techniques for the dynamical model parameters. They are the transient response method, the white noise excitation method, and the sinusoidal input signal method.

The first method uses a step-input signal for the system, and records the output transient response in time domain. The system parameters are found from the peak value, transient time and periodical time of the curve. This method is useful for the first and second order system. For a second order system it is desirable that the transient response be both sufficiently fast and damped.

For the sinusoidal excitation method, a constant amplitude input signal with variable frequency is used to excite the system. The output magnitude and phase angle are continuously recorded and drawn with the frequency as the parameter. From this bode diagram, the number of mode for this system can obtained. But it is difficult to distinguish mode shape (natural frequency, damping ratio) and the model parameters.

In the white noise excitation method, a limited bandwidth white noise with flat magnitude is applied to the system. The obtained time domain output signal is analyzed either through the FFT method to obtain the Bode diagram, or from the ARMA model to find the parameters of the difference equation by the stochastical regression method.

Among these identification methods, the latter one is very useful to directly obtain system parameters with a strong theoretical background. However the optimization search problem for the proper order of the model and the difficulty of transferring the higher order difference equation into the continuous model with meaningful physical explanation limit its practice.

1. Boring bar model

The mechanical dynamic model of the boring bar is built on a second order linear equation, since its component contains mass, spring and damper.

During the identification experiment, a white noise from the function generator with an amplitude of 1 volt and a bandwidth of 500 Hz is applied to the power amplifier. The latter is connected to the piezoelectric actuator and excites the boring bar.

The output displacement of the strain gauge sensor is sampled at 0.5ms. These data are fitted with an ARMA(2,1)model, which can be written as:

$$x_n - \phi_1 x_{n-1} - \phi_2 x_{n-2} = a_n - \theta_1 a_{n-1} \qquad (6\text{–}1)$$

where ϕ_1 — Autoregressive parameter

ϕ_2 — Autoregressive parameter

θ_1 — Moving average parameter

We can obtain:

ϕ_1=0.7575

ϕ_2=0.6874

θ_1=0.2743

The above equation is hoped to be converted to the equivalent continuous equation and to find out the parameters with the following form [You87]

$$\frac{d^2x(t)}{dt^2} + 2\xi\omega_n \frac{dx(t)}{dt} + x(t) = Z(t) \qquad (6\text{–}2)$$

where (t) — the output of the boring bar system

$Z(t)$ — the white noise

ξ — the damp ratio

ω_n — the resonance frequency

Since the autocovariance of the continuous output signal X(t) at the sampled points is a linear combination of two exponentials, it has the same form as that of the ARMA(2,1) model. It means that the following relations are applicable

$$\phi_1 = \lambda_1 + \lambda_2 = e^{\mu_1 \Delta} + e^{\mu_2 \Delta} \tag{6–3}$$

$$\phi_2 = -\lambda_1 \lambda_2 = -e^{(\mu_1 + \mu_2)\Delta} \tag{6–4}$$

and

$$\mu_1, \mu_2 = -\xi\,\omega_n \pm \omega_n \sqrt{1-\xi^2} = -A \pm iB$$

where λ_1 λ_2 — characteristic roots of the discrete model

μ_1 μ_2 — characteristic roots of the continuous model

Δ — sampling interval

Since $\phi_1^2 + 4\phi_2 < 0$

From the above equation, A and B can be expressed as

$$A = \xi\,\omega_n = -\frac{\ln(-\phi_2)}{2\Delta} = 375$$

and

$$B = \frac{-\ln(-\phi_2)}{2\Delta}\sqrt{-\left(\phi_1^2 + 4\phi_2\right)}\left[\frac{2\phi_1 - (1-\phi_2)\left(\theta_1 + 1/\theta_1\right)}{2\left(1-\phi_2^2\right) - \phi_1(1+\phi_2)\left(\theta_1 + 1/\theta_1\right)}\right] = 2450$$

with the above two equations and obtained discrete parameters, the continuous parameters ξ andω_n are calculated as

$$\omega_n = \sqrt{A^2 + B^2} = \sqrt{375^2 + 2450^2} = 2478 \tag{6–5}$$

$$\xi = \frac{A}{\omega_n} = \frac{375}{2478} = 0.15 \tag{6–6}$$

The transfer function representation between the output displacement and input force of the stage is thus expressed by

$$G_c(s) = \frac{1}{\left(\frac{s}{\omega_n}\right)^2 + 2\left(\frac{\xi}{\omega_n}\right)s + 1} = \frac{1}{\left(\frac{s}{2478}\right)^2 + \left(\frac{s}{8260}\right) + 1} \tag{6–7}$$

2. Piezoelectric actuator model

As described before, the actuator output and input relation can be roughly expressed by a constant gain element. However looking at the precision positioning requirement, its hysteresis appears to be undesirable. The canter position, the magnitude and the shape of the hysteresis are dependent on the applied input voltage magnitude and frequency.

Since the natural frequency of the actuator is 30 KHz, which is well above the tool drive requirement, its effect is neglected. Hence the simple relationship between the output displacement D(t) and input voltage V(t) is written as

$$G_a(s) = \frac{D(s)}{V(s)} = \frac{9}{50} \tag{6–8}$$

3. Power Amplifier Model

As mentioned before, the maximum operating frequency of the amplifier is a function of the output voltage amplitude. Generally the power amplifier has a linear behavior under a bandwidth of 120 Hz and an output voltage of 100 volts.

A simplified constant gain is also used to represent the amplifier model with the relationship between the output voltage $V_{out}(t)$ and input voltage $V_{input}(t)$

$$G_p(s) = \frac{V_{out}(s)}{V_{in}(s)} = \frac{100}{10} = 10 \tag{6–9}$$

4. Low pass filter model

The transfer function of the Low Pass Filter Model is of the form:

$$G_f(s) = \frac{V_0}{V_i} = \frac{1}{\left(\frac{s}{\omega_c}\right)^2 + 1.414\left(\frac{s}{\omega_c}\right) + 1}$$

where ω_c is the cut-off frequency of the filter, and $\omega_c = 2\pi f_c = 753$.

So we can obtain

$$G_f(s) = \frac{1}{\left(\frac{s}{753}\right)^2 + \left(\frac{s}{533}\right) + 1} \tag{6–10}$$

5.3 Optimization of Error Model

This section deals with the optimization of the error model. A series of

deflection errors of the boring bar have been obtained with a 400rpm spindle speed, a 12mm/min feed-rate and a depth of cut of 0.15mm.

By using the software of MINITAB, the order of the AR model was off-line decided. AR and ARMA models have been successively fitted to the data. The AR models are fitted from AR(1) to AR(10), and the ARMA models were fitted from ARMA(2,1) to ARMA(6,5).

The summary of the results for each AR and ARMA model is shown in Fig.5.2. It can be seen that the AIC value decreases as the order of the AR model increases until the adequate model is reached. Therefore, the adequate model for AR modeling is an AR(3) based on 400 data points. For the ARMA models, the AIC value shows that an ARMA(3,2) is an adequate model. In this research, the AR(3) model is employed for the boring errors.

Once the error and error model are obtained, the future error values can be forecasted based on the current and past data. The forecasting simulation was performed. The forecasted values were subsequently compared with the true error data to estimate the forecasting error. The simulation result is shown in Fig. 5.3. It is indicated that the forecasting errors are distributed normally and that the error model can forecast the boring error effectively.

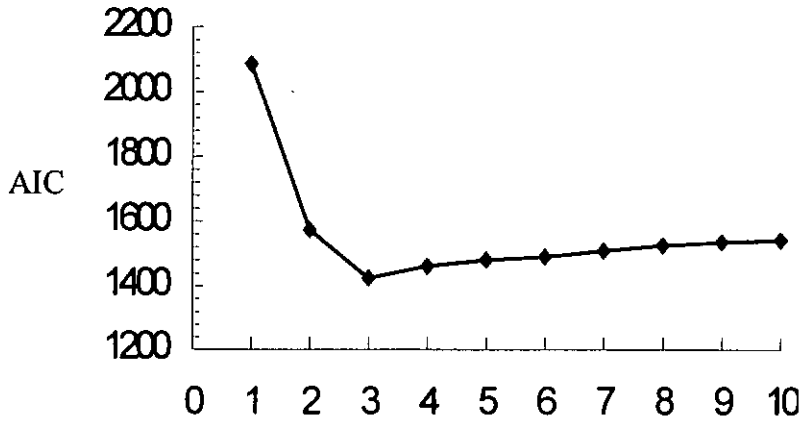

(a) AR (n) model

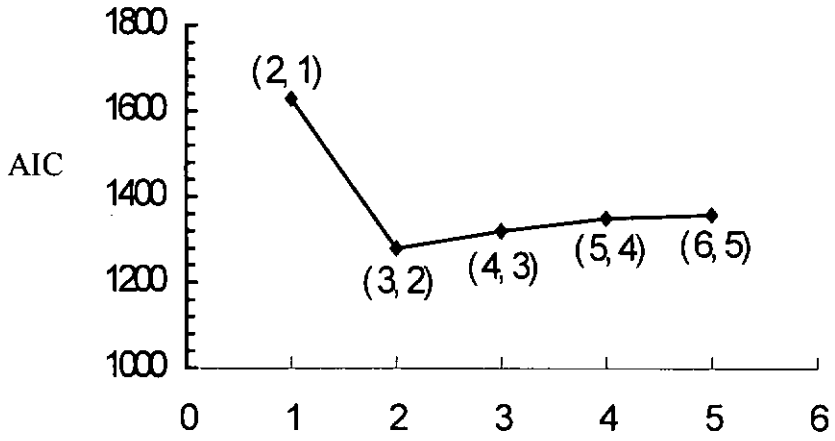

(b) ARMA (n, m)

Fig. 5.2 AIC values of AR(n) and ARMA(n, m) model

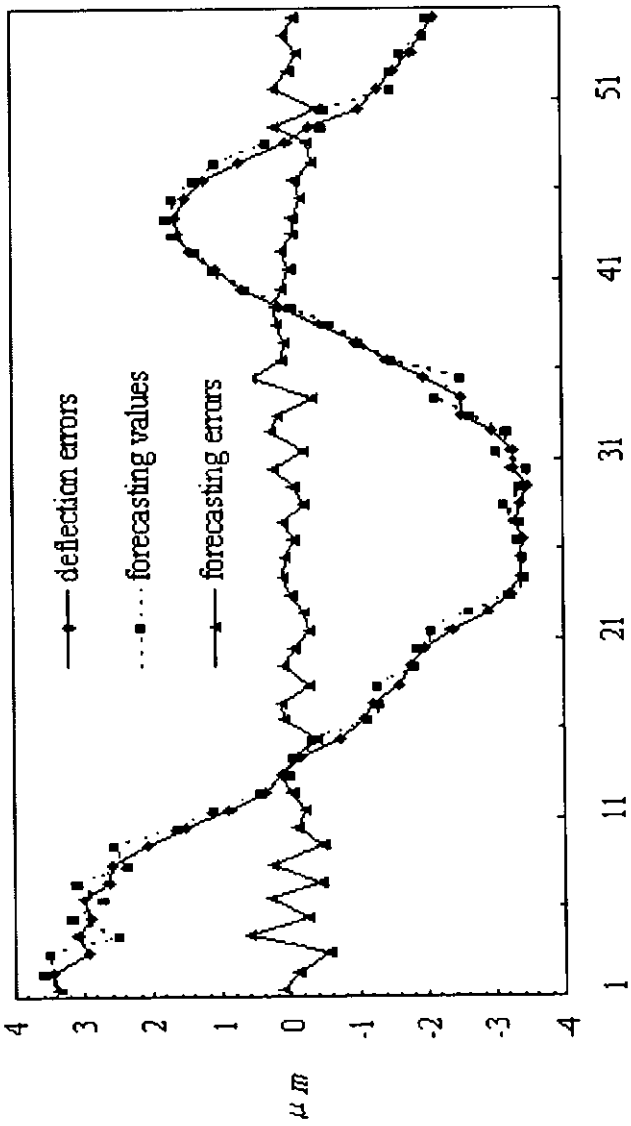

Fig. 5.3 The forecasting result of the AR(3) model

5.4 Software Programming

The software is written in Turbo C++. The programs are used for data acquisition through the ADDA converter card, reading and storing data, analysis of the input and output data, calculations and counter controls. The flowchart of program of the FCC algorithm is shown in Fig. 5.4.

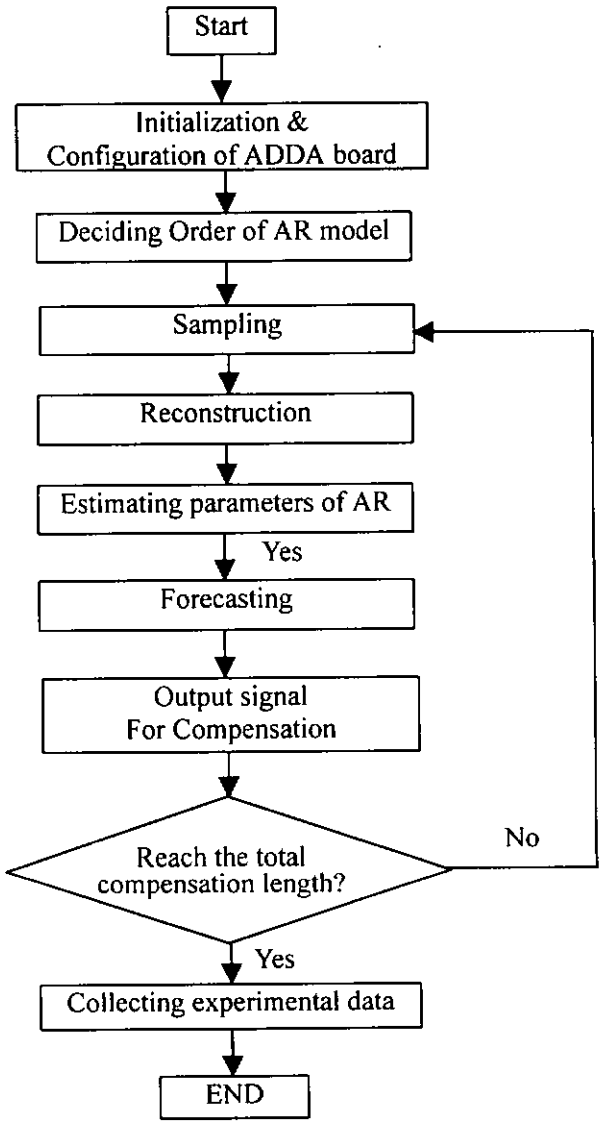

Fig. 5.4 The brief flow chart of the software system

5.5 Control Simulation

Based on the control algorithm described in previous section, an off-line cutting simulation experiment was conducted to check the validity of the control system. The apparatus set-up is shown in Fig.5.5. In the experiment, a sine wave input force was fed to push the cutting tool of the boring bar. The amplitude of the input force was made to a value at which the tool tip displacement was 2 μm . The frequency of the sine-wave signal changed from 5Hz to 40Hz. The displacements of the boring cutter are recorded by an oscillograph with and without compensation control. The simulation experimental result is shown in Fig. 5.6. It is indicated that the vibration of the boring cutter with frequency below 40 Hz can be suppressed effectively through the developed compensation algorithm.

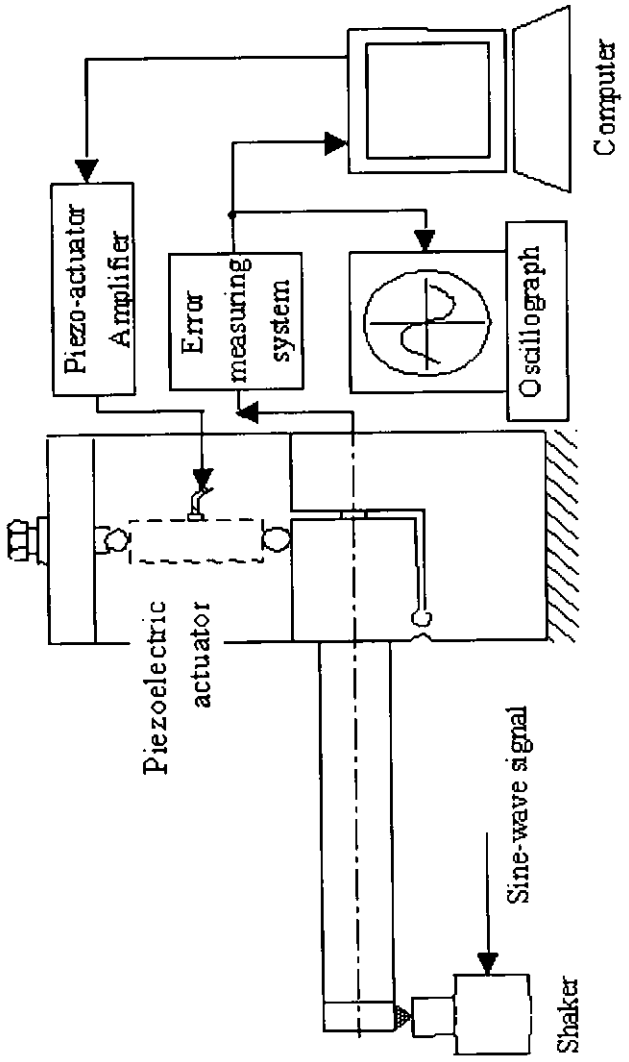

Fig. 5.5 The sketch of the cutting simulation experiment apparatus

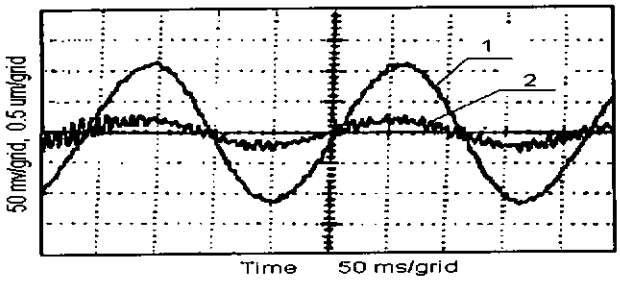

(a) 5Hz

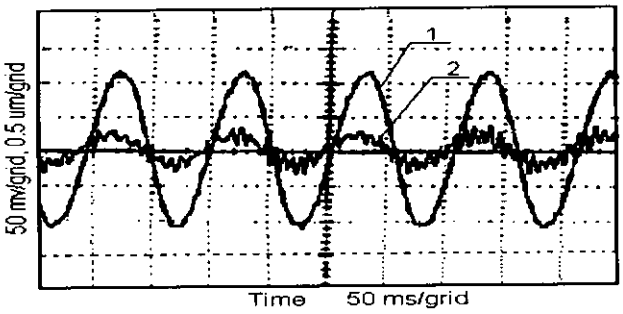

(b) 10Hz

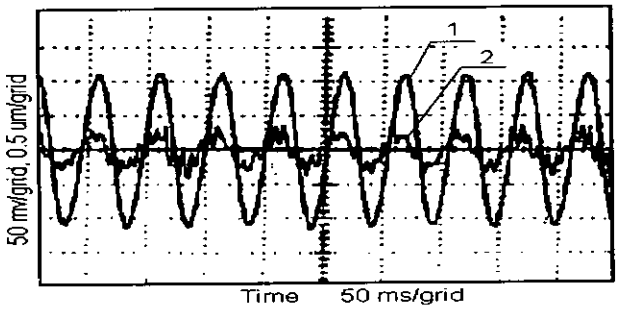

(c) 20Hz

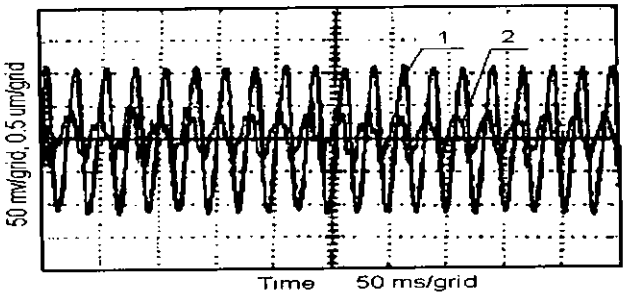

(d) 40Hz

Fig. 5.6 The simulation result of the micro-boring system

Chapter Six

ON-LINE CUTTING EXPERIMENTS

On-line cutting experiments were conducted to verify the ability of the proposed FCC system to compensate for the machining errors in boring operation. Section 6.1 presents the experiment of cutting workpieces with taper, which was performed to test the function of compensating the roundness errors and cut-depth errors of the proposed boring system. Section 6.2 gives the experiment of cutting workpieces with eccentricity, which was to identify the dynamic performances of the compensation system.

6.1 Cutting Workpiece with Taper Hole

6.1.1 Preparation of cutting experiments

Before the on-line cutting tests with the FCC scheme were made, some preparations were made and adjustments were performed to ensure that the whole system worked properly. These included tool preparation, actuator system adjustment, and preparation and calibration of the instruments, machine and workpiece.

(1) Preparation of the tool

Because of availability and for the purpose of simplicity, a carbide tool was selected for this study. The selected tool geometry is shown in Fig. 6.1. The size

of the boring tool is A=6.35mm, T=2.38mm, R=0.05mm.

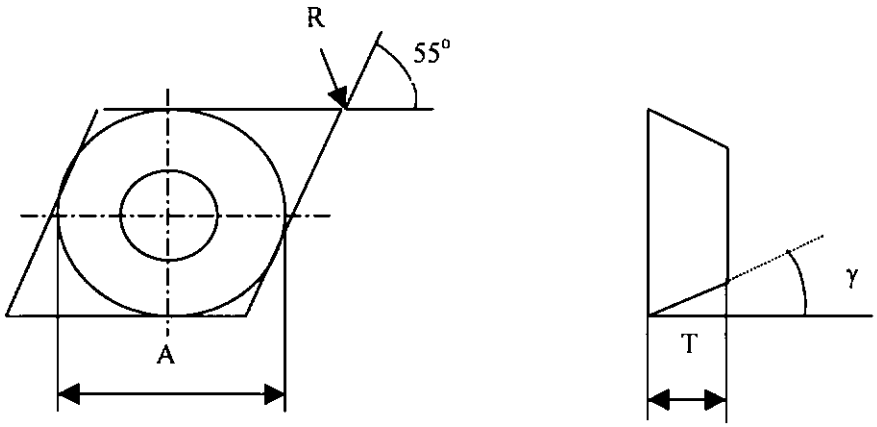

Fig. 6.1 The boring tool geometry

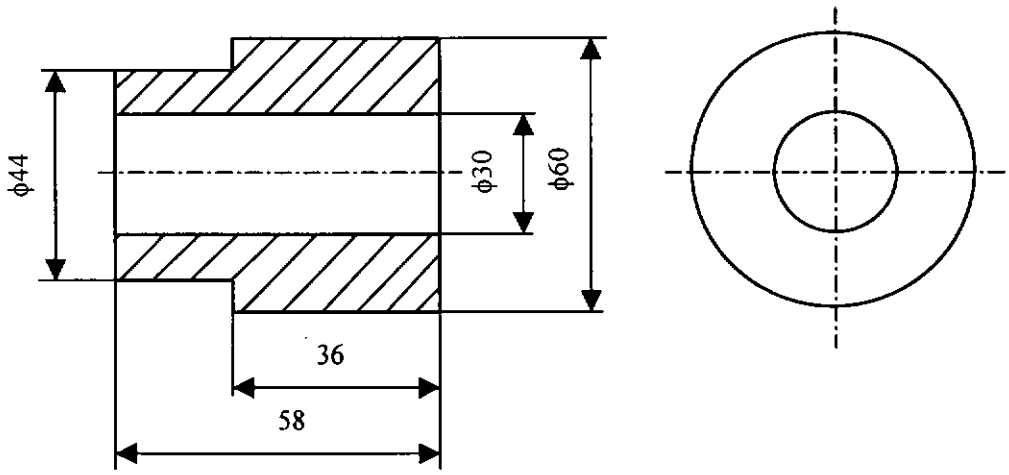

Fig. 6.2 The designed workpiece

(2) Preparation of instruments, machine and workpiece

To some extent, the instability of the instruments and of the machine is unavoidable due to temperature changes. In order to reduce this effect, the instruments and machine were warmed up for more than half an hour before starting the experiment for approaching the thermal equilibrium. The workpiece (see Fig. 6.2), which was made of aluminum, was carefully mounted on the 3-Jaw chuck of the CNC turning machine with moderate clamping force to minimize the deformations.

6.1.2 Experimental procedure

(1) Rough cut

A rough cut was conducted to eliminate the eccentricity between the workpiece and spindle due to the mounting error, and to cut off any irregular shape in the bore of the workpiece. This cut would normally precede the finishing cut in an actual boring operation.

(2) Taper cut

A taper cut was conducted to make a gradual increase in the depth of cut for the final finishing cut performed in the next step. Three samples were made. Out of these three, two samples were 0.33° tapered as (a) in Fig. 6.3 and one was 0.66° tapered as (b) in Fig.6.3.

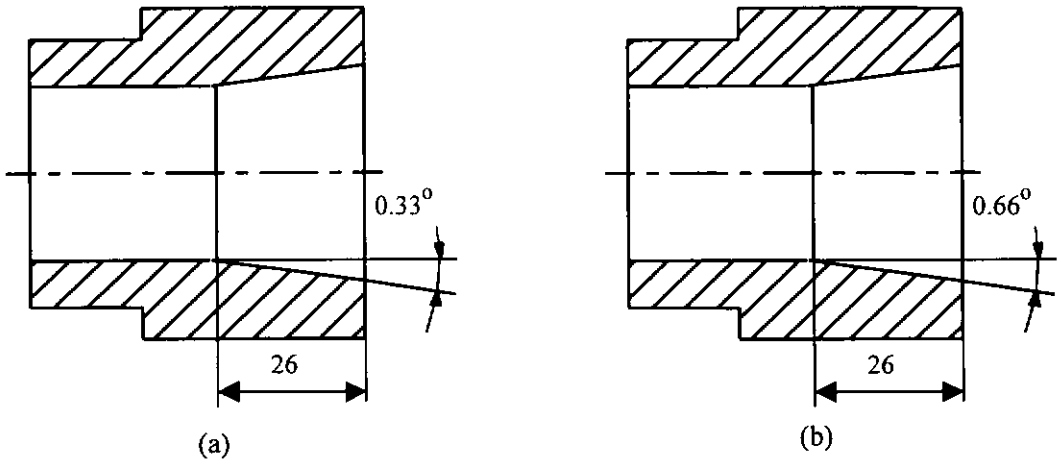

Fig. 6.3 The workpiece with taper-cut

(3) Finishing cut with and without compensation

A straight boring cut with 0.1mm and 0.3mm depths of cut were made in the samples with a 0.33° taper and 0.66° taper respectively. The cutting conditions were as follows: Spindle Speed was 600rpm, Feed-rate was 10mm/min.

During this cut, the cutting depths were gradually increased and the cutting tool error data were fetched by the personal computer, any tool tip displacement was compensated by bending the boring bar holder according to the FCC controller output. The compensation signal issued to the piezoelectric tool actuator system was nearly instantaneous with any error signal from the strain gauges sensing system.

(4) Measurement of workpiece sample error in diameter and roundness

The cut workpieces were measured on a Coordinate Measuring Machine and

a Roundness Measuring Machine (Taylor Hobson Talyrond 30). The bore diameters of different sections, 6mm apart, was recorded and shown in the next section. The roundness traces of different sections measured by the Talyrond 30-PC is shown in the next section.

6.1.3 Summary of experimental results

This section presents the measuring results of the on-line cutting experiments: diameter and roundness.

(1) Diameter

The diameters of the bore in each samples were measured at 4 sections. Each section was 6mm apart (see Fig.6.4), and the measuring result is shown in table 6.1.

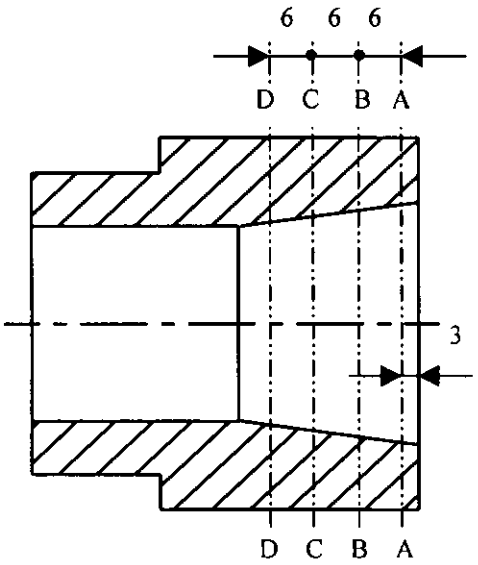

Fig. 6.4 The measuring sections of the workpiece

Table 6.1 Diameters for each section

mm

Section / Sample	A–A	B–B	C–C	D–D
Before Machining	30.265	30.196	30.127	30.058
Without Compensation	30.490	30.487	30.484	30.479
With Compensation	30.495	30.494	30.493	30.492

(2) Traces of roundness

The traces of roundness at the different sections of the bored hole were shown in Fig. 6.5, Fig.6.6, Fig. 6.7 and Fig.6.8. The result of the roundness was given in Table 6.2.

Table 6.2 Roundness for each section

μm

Section / Sample	A–A	B–B	C–C	D–D	Average
Without Compensation	6.55	7.60	6.45	6.00	6.65
With Compensation	4.05	4.00	4.20	3.85	4.03
Improvement	38%	47%	35%	36%	39%

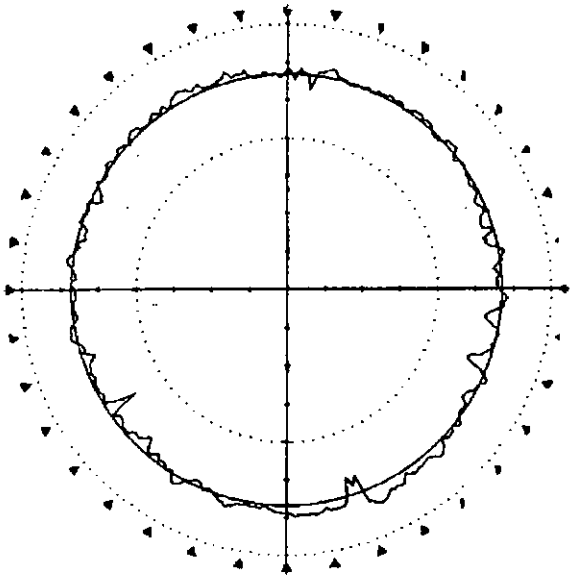

(a) Without compensation: roundness 6.55 μm

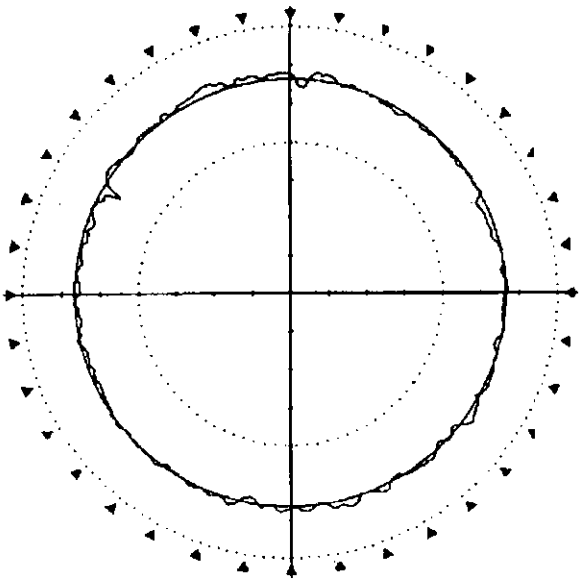

(b) With compensation: roundness 4.05μm

Fig. 6.5 The trace of roundness at A-A section

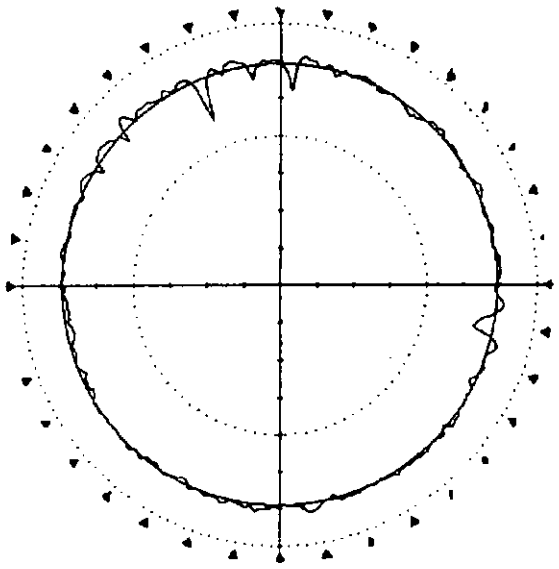

(a) Without compensation: roundness 7.60 μm

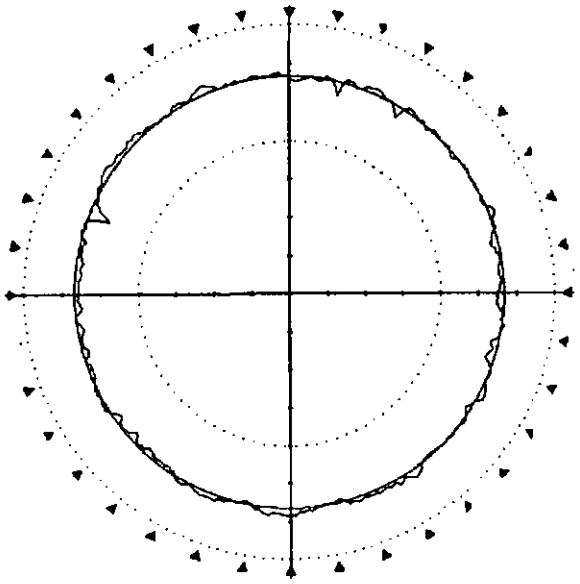

(b) With compensation: roundness 4.00 μm

Fig. 6.6 The trace of roundness at B-B section

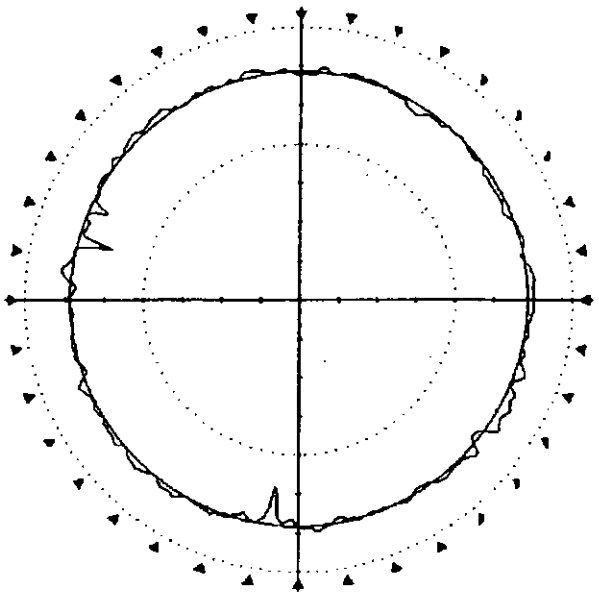

(a) Without compensation: roundness 6.45 μm

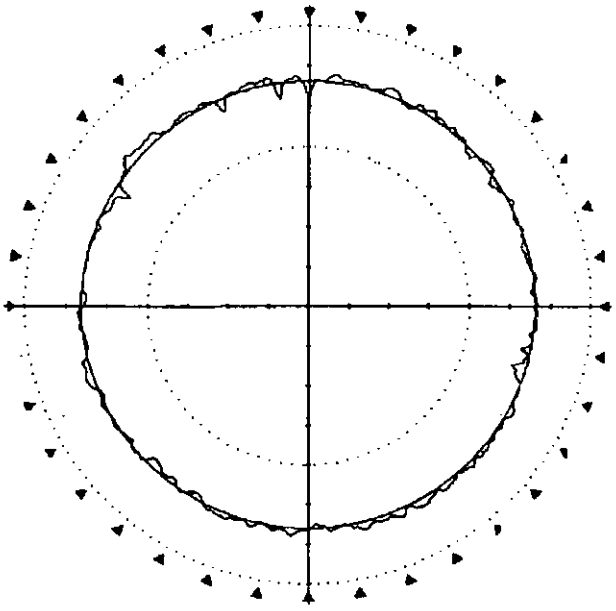

(b) With compensation: roundness 4.20 μm

Fig. 6.7 The trace of roundness at C-C section

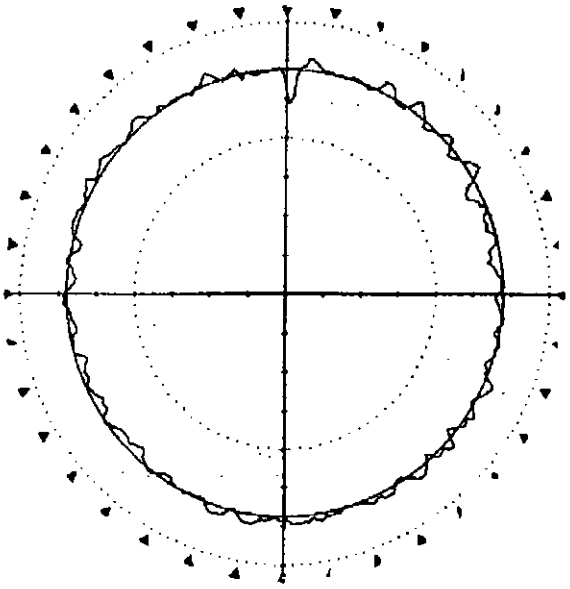

(a) Without compensation: roundness 6.00 μm

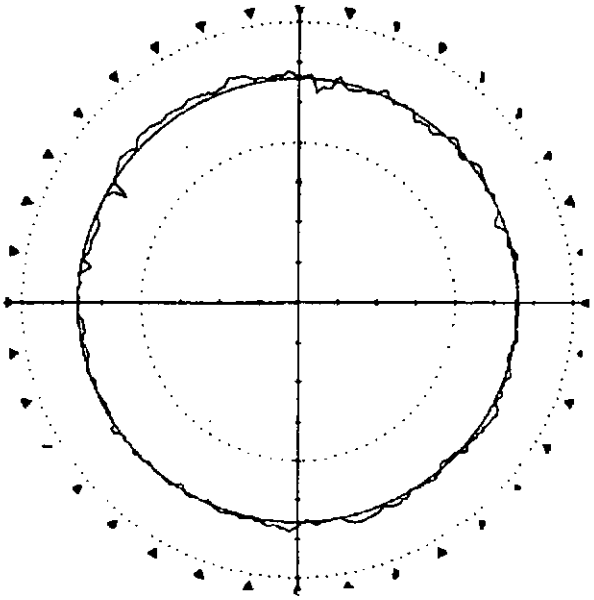

(b) With compensation: roundness 3.85 μm

Fig. 6.8 The trace of roundness at D-D section

6.1.4 Discussion of experimental results

From the experimental results presented in previous section, we can draw a graph as Fig. 6.9 and Table 6.3 to show the variations in diameters and depth of cuts after cutting respectively.

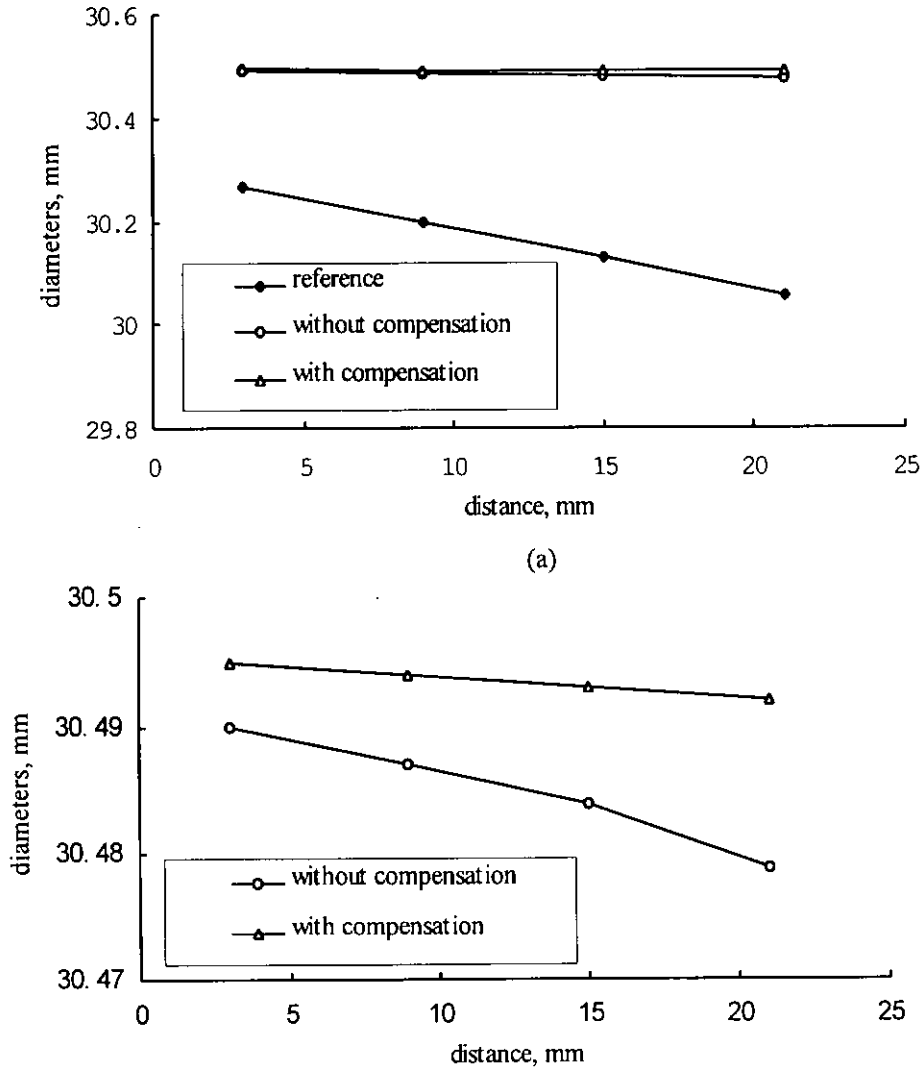

Fig. 6.9 The diameters for different section of the workpiece

Table 6.3 The cutting depths for each section mm

Section / Sample	A–A	B–B	C–C	D–D	Average
Theoretical value	0.235	0.304	0.373	0.442	——
Without compensation	0.225	0.291	0.357	0.421	0.324
With compensation	0.230	0.298	0.366	0.434	0.332
Error without Comp.	0.010	0.013	0.016	0.021	——
Error with Comp.	0.005	0.006	0.007	0.008	——
Improvement	50%	64%	56%	62%	56%

It is clear that the variations in diameter along the cutting path for the sample with compensation are much less than those for the sample without compensation (See Fig. 6.9). In other words, the sample with compensation has a more constant depth of cut than the sample without compensation. From the table 6.3, it is shown that the average improvement in cutting depth by the proposed system is about 56%

6.2 Cutting Workpiece with Eccentricity

In order to confirm the ability of the proposed FCC boring system to compensate for the machining error of different frequencies in boring operation, several workpieces with known eccentricities were cut in the condition of different spindle speeds. The roundness traces of the workpieces with compensation and without compensation were measured.

6.2.1 Preparation of workpiece with eccentricity

As shown in Fig. 6.10, the workpiece made of aluminum was used in this study. Firstly, the workpiece was amounted in the 3-jaw chucks, and was carefully bored. Secondly, a thin metal sheet with a thickness of 0.1mm was inserted between one jaw and the workpiece (see Fig. 6.11), and the workpiece was machined again. Then, the hole with an eccentricity was obtained due to the inserted sheet.

The eccentricity of the workpiece was measured by a micrometer which was installed to the base of the boring bar. It was found that the eccentricity of the workpiece was about 0.1mm, which was approximately equated to the thickness of the chip inserted.

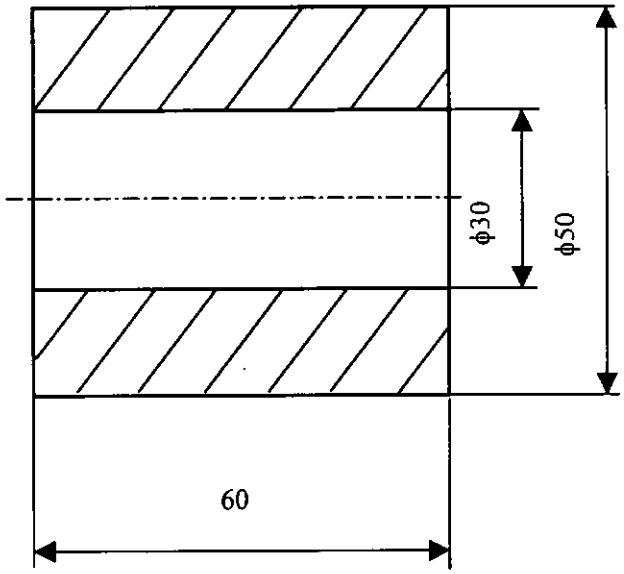

Fig. 6.10 The workpiece dimension

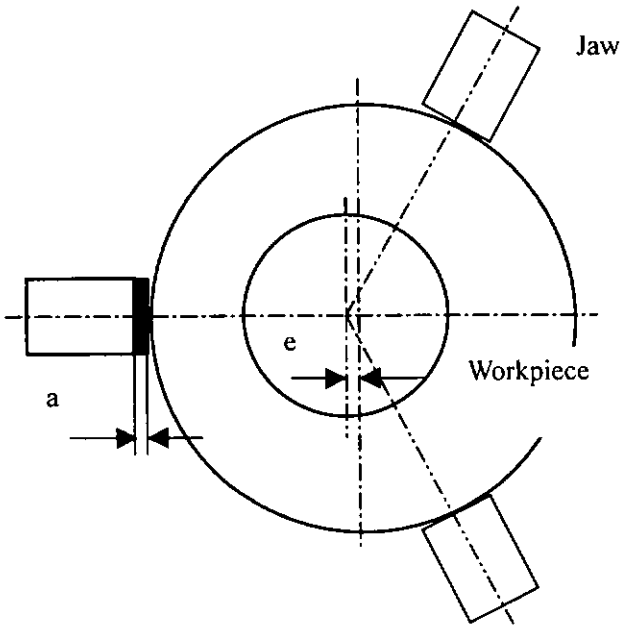

Fig. 6.11 The workpiece with an eccentricity

6.2.2 Experimental procedure

After preparation, the workpieces with eccentricity were bored in a CNC lathe. Each workpiece was bored at different spindle speeds ranging from 500rpm to 800rpm. Then, the workpieces were sent to a roundness measuring machine (Taylor Honbson Talyrond 30-PC) for measuring their profile traces.

6.2.3 Discussion of experimental results

Because of the eccentricity, the cutting depth changed during the cutting process, and the changing frequency was proportional to the spindle speed of the CNC lathe. The roundness trace measuring results of workpieces with different spindle speeds are shown in Fig. 6.12, Fig. 6.13, Fig. 6.14 and Fig. 6.15 respectively, and (a) shows the roundness trace of the workpiece machined without compensation, while (b) shows the roundness trace with compensation. It is clear that the roundness traces without compensation are elliptical and traces with compensation are more round. This indicates that the cutting depth error can be compensated efficiently by the developed FCC system during the boring operation.

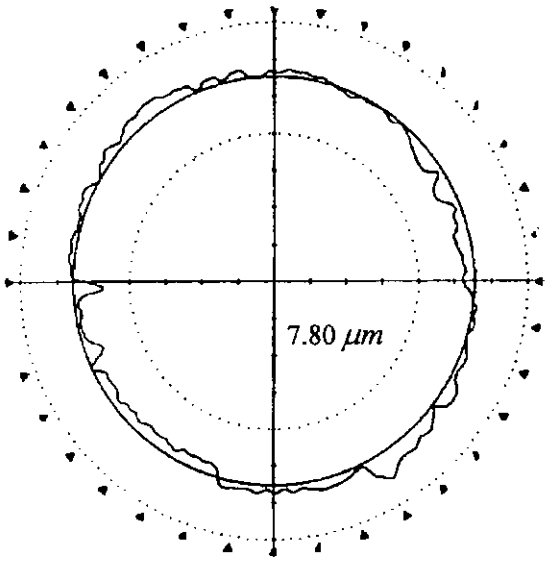

(a) Without compensation

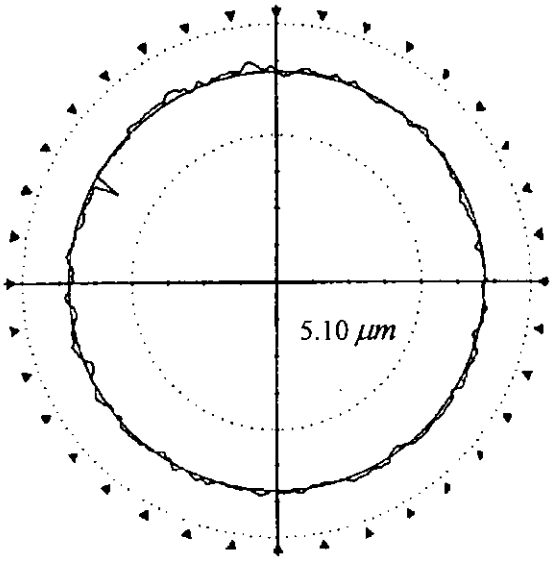

(b) With compensation

Fig. 6.12 The roundness trace at 500rpm

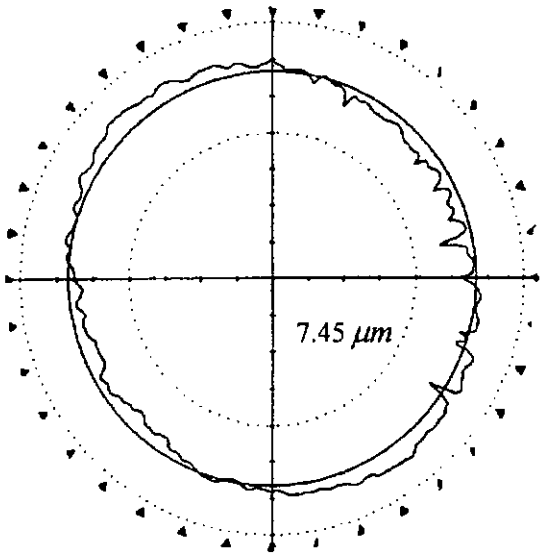

(a) Without compensation

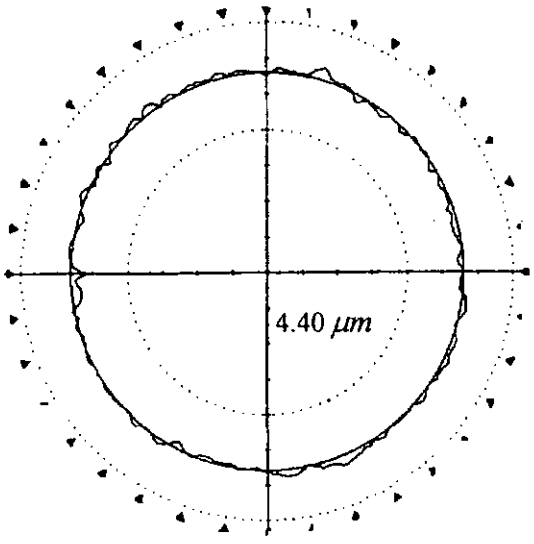

(b) With compensation

Fig. 6.13 The roundness trace at 600rpm

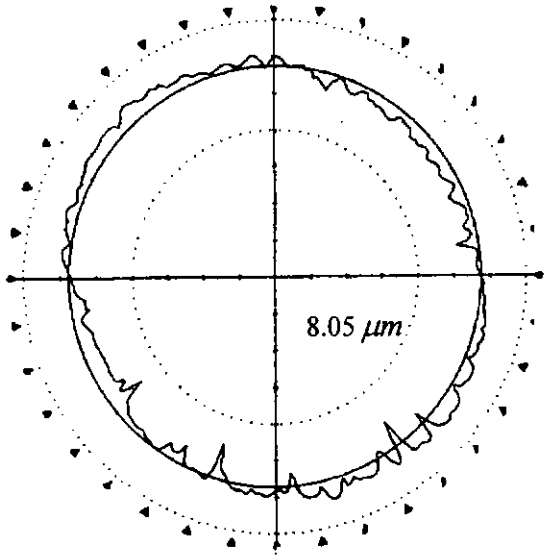

(a) Without compensation

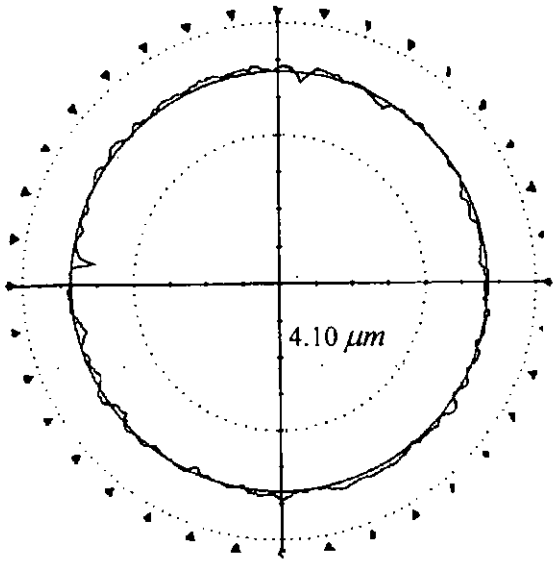

(b) With compensation

Fig. 6.14 The roundness trace at 700rpm

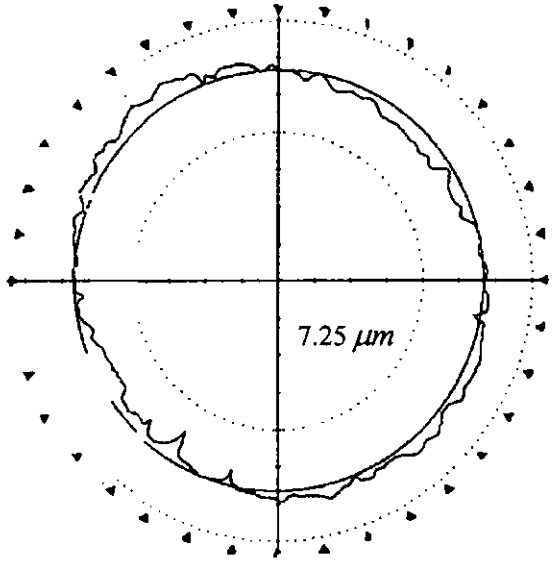

(a) Without compensation

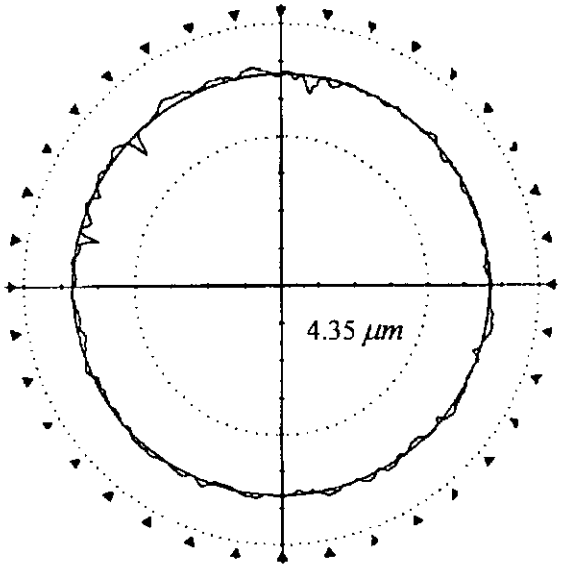

(b) With compensation

Fig. 6.15 The roundness trace at 800rpm

Chapter Seven

CONCLUSIONS AND FUTURE WORK

7.1 Conclusions

The purpose of this study was to develop a new on-line control scheme for improving the accuracy of small and deep hole boring operations. The on-line cutting results verify that a significant improvement of 39% of roundness and 60% of cutting depth accuracy was achieved by using the developed error compensation control system. The conclusions of previous chapters can be summarized as follows:

1. A boring bar with a new structure was developed. The boring bar was designed into the structure consisting of two coaxial bars. As a result, the micro-boring bar can be made with a relatively smaller outer diameter, which is suitable for the small and deep hole boring operation even the measuring and compensating sensors have been incorporated.

2. Strain gauges were employed to on-line measure the deflection errors of the cutter in the boring operation, since they can be installed into the boring bar without affecting its size. The measuring principle of strain gauge was studied, and the calibration experiment was conducted, which indicated that this indirect measuring method performed its function well.

3. A precision actuator system based on a piezoelectric translator was

designed. The system has a positioning accuracy of 0.08 micrometers and a dynamic response bandwidth of 80 Hz.

4. AR and ARMA models were fitted to the deflection errors during the boring operation. The AR(3) model were found to be an adequate model according to Akaike's Information Criterion.

5. A new control strategy, Forecasting Compensatory Control (FCC), which can compensate for both deterministic and stochastic errors, and overcome the time lag between the moment of measurement and that of tacking control action as well, was proposed to predict on-line and compensate the machining error during the boring process.

6. An off-line controller simulation study was carried out to verify the effectiveness of the proposed FCC algorithm. Furthermore, on-line cutting experiments were conducted to evaluate the effectiveness of the developed boring setup. It is indicated that the boring bar system can reduce the roundness error of the workpiece by 39%, and cutting depth error by 60%.

7.2 Future Works

The future work related to this project is suggested as follows:

1. Separating the errors of the workpieces from the errors of the spindle.

In recently years, a method of on-line measuring roundness and cylindricity of workpiece on a machine tool through application of a roundness measurement principle called the error separation method has been widely employed in the

precision turning operation. By this error separation method, roundness and cylindricity of workpieces can be obtained through being separated from the rotating error of the spindle and can be in-situ compensated. In the developed micro-boring system, the error signals detected by the strain gauges include both the errors of the workpiece and the rotating errors of the spindle. The machining accuracy would be improved more if the error separation method were used during the boring operation.

2. Improving the action frequency of the compensation system.

   The compensation frequency of the developed boring bar system is low because of the low resonant frequency of the boring bar with large length to diameter ratio. The resonant frequency of the boring bar can be increased by inserting some damping materials such as rubber into it, so that the compensation frequency can be improved for compensating the roughness errors.

3. Implementing the system into industry

   The ultimate purpose of the research is to apply the research results to industry. The developed micro-boring bar system should be modified for easier generation and to be operated easily and with greater stability for use in industry.

REFERENCES

[Asa92] Asao, T., Mizugaki, Y., and Sakamoto, M. "Precision turning by means of a simplified predictive function of machining error". *annals of the CIRP*, Vol. 41, No.1, pp.447-450 (1992)

[Au75] Au, Y. H. J. and New, R. W. "Cutting forces and tentative analysis of factors affecting geometric form and eccentricity of finished bores". *Proceedings of 3rd International Conference on Production Research,* Amherst, (1975)

[Box76] Box, G. E. P. and Jenkins, G. M. *Time Series Analysis—forecasting and control,* Holden Day, San Francisco, 575pp(1976)

[Cha93] Chan, K. W. "Development of a Zero Compliance Tool Holder for Precision Turning Machine". *Mphil dissertation of the Hong Kong Polytechnic University,* (1993)

[Che96] Chen, J. S. "Improving the Machine Accuracy Through Machine Tool Metrology and Error Correction". *Advanced Manufacturing Technology*, Vol. 11, pp.198–205(1996)

[Chi59] Chisholm, A. J., Lickley, M. and Brown J. P. *The Action of Cutting Tools*. Machinery Publishing Co., (1959)

[Chi95] Chiu, W. M. and Chan, K. W. "Design and Testing of Piezoelectric Controlled Boring Bar to Compensate for Cutting Force-Induced Errors in Variable Dept-of-Cut Conditions". *Proceedings of the 13th*

International Conference on Production Research, Jerusalem, Israel, August 6-10, (1995)

[Chi97] Chiu, W. M. and Chan, K. W. "Design and Testing of Piezoelectric Actuator-Controlled Boring Bar for Active Compensation of Cutting Force Induced Errors". *International Journal of Production Economics*, Vol. 51, pp.135–148 (1997)

[Don86] Donmez, M. A. and Blomquist, D. S. "A General Methodology for Machine Tool Accuracy Enhancement by Error Compensation". *Precision Engineering*, Vol. 8, No. 4, pp.187–196(1986)

[Fan91] Fan K. C. and Chao Y. H. "In-Process Dimensional Control of the Workpiece During Turning". *Precision Engineering*, Vol. 13, No.1, pp27–32(1991)

[Fer87] Ferreira, S. C., and Liu, C. R. "A Method for Estimating and Compensating Quasi-static Errors of Machine Tools." *ASME PED,* Vol. 27, pp205–229 (1987)

[Gra90] Granger C. "Compensating for Machine Errors". *Machinery and Production Engineering*, Vol. 148, pp. 60–64(1990)

[Gro80] Group, D., Jain, V. K. and Salaki, J. "A Comparative Analysis of Various Least-squares Identification Algorithm," *Automatica*, Vol. 16, pp.663-681 (1980)

[Han53] Hahn, R. S. "Solving Production Baoring Problems". *The Tool Engineer*, pp85–88 (1953)

[Han94] Hanson, R. D. and Tsao, T. C. "Development of a Fast Tool servo for Variable-Depth-of-cut Machining". *Dynamic Systems and Control, ASME,* DSC-Vol 55, No. 2, pp. 863–871(1994)

[Han98] Hanson, R. D. and Tsao, T. C. "Reducing Cutting Force Induced Bore Cylindricity Errors by Learning Control and Variable Depth of Cut Machining". *Transactions of the ASME, Journal of Manufacturing Science and Engineering*, Vol. 120, pp.547–552(1998)

[Har90] Hara,Y., Motonishi, S., and Yoshida, K. "A New Micro-cutting Device with High Stiffness and Resolution". *Annals of the CIRP*, Vol. 39, No. 1, pp.375–378 (1990)

[Hic67] Hicks, J. R., Raplay, L. A. And Islam M. R. "NC micro-boring by adaptive control." *Metalworking production*, pp60–63(1967)

[Hoc80] Hocken, R. J., "Machine Tool Accuracy," *Technology of Machine Tools,* The International Conference of the Machine Tool Task Force, Chicago, IL, Vol.5, pp8-60(1980)

[Hol95] Holman A. E. and Schoite, P. M. L. O. "Analysis of Piezo-Actuators in Translation Constructions". *Rev. Sci. Instrum.*, Vol. 66, No. 5, pp. 3208–3215 (1995)

[Ise74] Isermann, R. J. "Comparison of Six On-line Identification and Parameter Estimation Methods". *Automatica*, Vol. 10, pp. 81-103 (1974)

[Kan76] Kanai, A. and Suzuki, N. "The Development of the Load

Compensation for Cylindrical Grinding Machine". *Annals of the CIRP*, Vol. 25, No. 1, pp.313–318 (1976)

[Kat92] Katsuki, A., Onikura, H., Sajima, T. and Akashi, T., "Development of a deep-hole boring tool guided by laser". *Annals of the CIRP*, Vol. 41, No. 1, (1992)

[Kim86] Kim, K. "Forecasting Compensatory Control of Cylindricity in Contour Boring Operations". *Ph. D. thesis of The University of Wisconsin*, (1986)

[Kim87a] Kim, K., Eman, K. and Wu, S. M. "Development of a Forecasting Compensatory Control System for Cylindrical Grinding". *ASME Trans.* Vol. 109, pp.385–391(1987)

[Kim87b] Kim, K. "Cylindrical Accuracy Control Based on Stochastic Modeling and Forecasting Compensation". *International Journal of Machine Tools & Manufacturing*. Vol. 28, No. 4, pp.495-501(1988)

[Kim87c] Kim, K., Eman, K. F., and Wu, S. M. "In-Process Control of Cylindricity in Boring Operations". *Journal of Engineering for Industry*, Vol. 109, pp291-296 (1987)

[Kim88] Kim, K. "New Active Error Compensatory Method of Machinery Accuracy". *International Journal of Production Research*, Vol. 26, pp.1613–1618 (1988)

[Lec98] Lechniak, Z., Werner, A. and Skalski, K. "Methodology of Off-line Software Compensation for Errors in the Machining Process on the

CNC Machine Tool". *Journal of Materials Processing Technology*, Vol. 76, No. 1–3, pp.42–48(1998)

[Lee64] Lee, R. C. K. *Optimal Estimation, Identification and Control*, MIT Press, Cambridge, Mass., (1964)

[Li96] Li, C. J. "To Improve Workpiece Roundness in Precision Diamond Turning by In Situ Measurement and Repetitive Control". *Mechatronics*, Vol. 6, No.5, pp.523–535 (1996)

[Lia92] Liang S. and Perry S. "Milling Cutter Runout Compensation By Control of Radial Depth of Cut". *Japan/USA Symposium on flexible Automation*, Vol. 2, pp861–864 (1992)

[Lo95] Lo, C. H. and Ni, J. "an Application of Real-time Error Compensation on a Turning Center". *International Journal of Machine Tools & Manufacture*, Vol. 35, No. 12, pp.1669–1682(1995)

[Mou95] Mou, J. and Liu, C. R. "An Adaptive Methodology for Machine Tool Error Correction". *Journal of Engineering for Industry*, Vol. 117, pp. 389–399 (1995)

[Oka90] Okazaki, Y. "A Micro-Positioning Tool Post Using a Piezoelectric Actuator for Diamond Turning Machines". Precision Engineering Vol. 12, No. 3, 151–156 (1990)

[Ots89] Otsuka, J. "Precision Thread Grinding Using a Laser Feedback System". *Precision Engineering*, Vol. 11, No. 2, pp.89–93 (1989)

[Pan83] Pandit, S. M. and Wu, S. M. *Time Series and System Analysis with*

Applications, Wiley, New York, 585pp (1983)

[Par65] Paros, J. M. and Weisbord, L. "How to Design Flexure Hinges". *Machine Design*, Vol. 37, No. 27, pp.151–156 (1965)

[Par88] Park, C. W., Eman K. F. and Wu, S. M. "Forecasting Compensatory Control of Machining Flatness". *International Journal of Machine Tools and Manufacturing*, Vol. 28, No. 1, pp.59–67 (1988)

[Pat85] Patterson, S. R. and Magrab, E. B. "Design and Testing of a Fast Tool servo for Diamond Turning". *Precision Engineering,* Vol. 7, No. 3, pp.123–128 (1985)

[Rao82] Rao, S. B and Wu, S. M. "Compensatory Control of Roundness Error in Cylindrical Chuck Grinding". *ASME Trans.*, Vol. 104, pp.23–28 (1982)

[Ras92] Rasmussen, J. D, Tsao, T. C., Hanson, R. D. and Kapoor, S. G. " A piezoelectric Tool Servo System for Variable Depth of Cut Machining". *ASME PED*, Vol. 58, pp119-130 (1992)

[Ras94] Rasmussen, J. D. "A Piezoelectric Tool Servo System for Variable Depth of Cut Machining". *International Journal of Machine Tools & Manufacturing*, Vol. 34, No. 3, pp.379–392(1994)

[Riv86] Rivin, E. I. "Structural Optimization of Cantilever Mechanical Elements". *Journal of Vibration, Acoustics, Stress, and Reliability in Design*, Vol. 108, pp.427–433 (1986)

[Riv89] Rivin, E. I. "Improving Dynamic Performance of Cantilever Boring

Bars". *Annals of the CIRP*, Vol. 38, No. 1, pp.377-380 (1989)

[Sar76] Sarids, G. N., "Comparison of Six On-line Identification Algorithms," *Automatica*, Vol. 10, pp. 93-99 (1976)

[Shi79] Shiraishi M. "In-Process Control of Workpiece Dimensions in Turning". *Annals of the CIRP*, Vol. 28, No. 1, pp.333–337 (1979)

[Sho98] Showky, A. M. and Elbestawi, M. A. "Model-Based Predictive Control of Workpiece Accuracy in Bar Turning". *Transactions of the ASME, Journal of Manufacturing Science and Engineering,* Vol. 120, No. 1, pp.57–67 (1998)

[Sub93] Subramani, G., Kapoor, S. G. and Devor, R. E. "A Model for the Prediction of Bore Cylindricity During Machining". *Journal of Engineering for Industry*, Vol. 115, 15–22 (1993)

[Tan94] Tanaka, H., Obata, F., and Matsubara T. "Active Chatter Suppression of Slender Boring Bar Using Piezoelectric Actuators". JSME International Journal, Series C, Vol. 37, No. 3, pp.601–606 (1994)

[Tew95] Tewani, S. G., Rouch, K. E. and Walcott, B. L. "A Study of Cutting Process Stability of a Boring Bar with Active Dynamic Absorber". *International Journal of Machine Tools & Manufacturing,* Vol. 35, No. 1, pp.91–108 (1995)

[Win82] Windows, A. L. *Strain Gauge Technology,* London Applied Science, (1982)

[Wu89] Wu, S. M., and Ni, J. "Precision Machining without Precision Machinery". *Annals of the CIRP*, Vol.38, No. 1, pp.533–536 (1989)

[You87] Your S. B. "Precision Control on the Winchester Disc Flatness in Face-Turing Operations". *Ph. D thesis of The University of Wisconsin.* (1987)